Dynamically regularized Lagrange multiplier schemes with energy dissipation for the incompressible Navier-Stokes equations

Cao-Kha Doan[a], Thi-Thao-Phuong Hoang[a,*], Lili Ju[b], Rihui Lan[c]

[a] *Department of Mathematics and Statistics, Auburn University, Auburn, AL 36849, USA*
[b] *Department of Mathematics, University of South Carolina, Columbia, SC 29208, USA*
[c] *School of Mathematical Sciences, Ocean University of China, Qingdao 266100, China*

Abstract

In this paper, we present efficient numerical schemes based on the Lagrange multiplier approach for the Navier-Stokes equations. By introducing a dynamic equation (involving the kinetic energy, the Lagrange multiplier, and a regularization parameter), we form a new system which incorporates the energy evolution process but is still equivalent to the original equations. Such nonlinear system is then discretized in time based on the backward differentiation formulas, resulting in a dynamically regularized Lagrange multiplier (DRLM) method. First- and second-order DRLM schemes are derived and shown to be unconditionally energy stable with respect to the original variables. The proposed schemes require only the solutions of two linear Stokes systems and a scalar quadratic equation at each time step. Moreover, with the introduction of the regularization parameter, the Lagrange multiplier can be uniquely determined from the quadratic equation, even with large time step sizes, without affecting accuracy and stability of the numerical solutions. Fully discrete energy stability is also proved with the Marker-and-Cell (MAC) discretization in space. Various numerical experiments in two and three dimensions verify the convergence and energy dissipation as well as demonstrate the accuracy and robustness of the proposed DRLM schemes.

Keywords: Incompressible Navier-Stokes equations; Energy stability; Lagrange multiplier; Dynamic regularization; Marker-and-Cell method

1. Introduction

The incompressible Navier-Stokes (NS) equations are fundamental in computational fluid dynamics, governing the behavior of incompressible fluid flows. In this paper, we study these equations in the following form:

$$\begin{cases} \boldsymbol{u}_t - \nu\Delta\boldsymbol{u} + \boldsymbol{F}(\boldsymbol{u}) + \nabla p = \boldsymbol{f}, & \text{in } \Omega\times(0,T], \quad (1.1a) \\ \nabla\cdot\boldsymbol{u} = 0, & \text{in } \Omega\times(0,T], \quad (1.1b) \end{cases}$$

subject to the initial condition $\boldsymbol{u}(\boldsymbol{x},0) = \boldsymbol{u}_0(\boldsymbol{x})$ and the homogeneous Dirichlet or the periodic boundary condition. In (1.1), Ω is an open bounded domain in $\mathbb{R}^d$ ($d = 2, 3$), $\boldsymbol{u} = (u_1, \ldots, u_d)^T$

*Corresponding author
Email addresses: kcd0030@auburn.edu (Cao-Kha Doan), tzh0059@auburn.edu (Thi-Thao-Phuong Hoang), ju@math.sc.edu (Lili Ju), lanrihui@ouc.edu.cn (Rihui Lan)

and p are the unknown velocity field and pressure respectively, $\boldsymbol{F}(\boldsymbol{u}) = (\boldsymbol{u} \cdot \nabla)\boldsymbol{u}$ denotes the nonlinear convection, $\boldsymbol{f}$ is an external force, and ν represents the kinematic viscosity which is inversely proportional to the Reynolds number Re. It is well known that, in the absence of external forces, the incompressible NS equations (1.1) under the prescribed boundary conditions satisfy the energy dissipation. Therefore, it has been highly desirable to develop numerical schemes for (1.1) that preserve this key property.

Projection methods, originally proposed by Chorin [8] and Temam [34], are among the most commonly used methods for solving the incompressible NS equations (1.1). These methods consist of a prediction step for the velocity and a projection step to enforce the incompressible condition (1.1b) at each time step. However, one needs to introduce artificial boundary conditions for the pressure, leading to boundary layers and reducing its convergence rates [38, 12]. To overcome such issues, in [29, 39, 40] the gauge formulation was developed by using the Helmholtz-Hodge decomposition to rewrite (1.1) in terms of two auxiliary variables, the vector variable $\boldsymbol{a}$ and the scalar variable ϕ, for which $\boldsymbol{u} = \boldsymbol{a} + \nabla\phi$ and $\boldsymbol{u}$ is orthogonal to $\nabla\phi$. A key advantage of this formulation is the flexibility in choosing suitable boundary conditions for the nonphysical variable ϕ. Although the gauge formulation can be easily combined with traditional time discretization methods (e.g., backward Euler and Crank-Nicolson schemes [36, 27]) as well as more advanced approaches (e.g., exponential time differencing methods [19]), achieving energy stability for the resulting schemes remains challenging.

Motivated by the invariant energy quadratization (IEQ) methods [42, 46, 43, 45], the scalar auxiliary variable (SAV) schemes have recently been developed for simulating gradient flows [32, 33, 18, 1, 35, 7], in which time-dependent auxiliary variables are introduced to transform the free energy into a quadratic form, allowing for an explicit treatment of nonlinear terms. The SAV schemes are shown to be unconditionally energy stable (usually with respect to certain modified energies), provided that the nonlinear part of the free energy is bounded from below. Such a boundedness requirement is automatically satisfied by the incompressible NS equations (1.1), thus in [24] an auxiliary variable associated with the total system energy of (1.1) was introduced to reformulate the NS equations into an equivalent system with an extra dynamic equation for the auxiliary variable. The resulting linear schemes are unconditionally energy diminishing, marking the first time that numerical schemes with explicit treatment of the nonlinear convection term can preserve this important property. Following this idea, a second-order in time numerical scheme for the NS equations was constructed based on the SAV approach for time stepping and the Marker-and-Cell (MAC) method for spatial discretization in [22], where the auxiliary variable is computed via a quadratic equation at each time step. Later in [23], new SAV-pressure correction methods were introduced where only a linear algebraic equation needs to be solved for the scalar variable, whose exact value is an exponential decay function. Besides the SAV approach, it is well known that the Lagrange multiplier technique also helps lead to unconditionally energy stable schemes. Inspired by [6], in [44] a Lagrange multiplier was introduced into a dynamic equation for the original kinetic energy, and the proposed second-order backward differentiation formula (BDF) scheme was shown to satisfy energy stability that involves the original energy and some pressure gradient terms.

Although both SAV and Lagrange multiplier approaches are efficient to implement, requiring only the solutions of generalized Stokes systems (for the coupled approach) or a sequence of Poisson-type equations (for the decoupled approach) at each time step, they usually pose three challenges: (i) Solving nonlinear algebraic equations for the Lagrange multiplier is required at each time step, which may produce multiple real or even complex solutions; (ii) To maintain accuracy for the

SAV and Lagrange multiplier methods, especially the latter, the time step size must be sufficiently small, which is not efficient in terms of computational cost for long-term simulations; (iii) Most stability results from the SAV methods concern a modified energy, which is not directly related to the original energy. Thus, the boundedness of the original energy is not straightforwardly implied, especially when large time step sizes are applied.

In this paper, we aim to develop a novel class of numerical schemes, namely *dynamically regularized Lagrange multiplier* (DRLM) schemes, for the incompressible NS equations to overcome the aforementioned challenges. Partially motivated by recent work [15] for gradient flows, we first reformulate the model problem (1.1) into an equivalent system that includes an additional dynamic equation involving the kinetic energy, a Lagrange multiplier, and a positive regularization parameter. First- and second-order DRLM schemes are then obtained by using the BDF methods with an explicit treatment of the nonlinear convection term. These schemes are shown to be unconditionally energy stable with respect to the original variables. Fully discrete energy stability is also proved with the MAC discretization in space. While our stability analysis also concerns a modified energy consisting of the original energy plus an error evolution term for the Lagrange multiplier, numerical results show that the modified energy is almost identical to the original energy (cf. Remark 3.1(i) and Section 4), even when the regularization parameter is large. The proposed schemes are linear and simple to implement, requiring only the solutions of two generalized Stokes systems and a scalar quadratic equation at each time step. Note that each Stokes system can be replaced by two Poisson-type equations if one considers the pressure-correction approach [12, 13] for the DRLM formulation (cf. Remark 2.3). Importantly, unlike existing Lagrange multiplier schemes [44], we observe that the proposed DRLM schemes can guarantee the uniqueness of the discrete Lagrange multiplier (and consequently the unique solvability of the numerical solutions) by choosing a sufficiently large regularization parameter, especially when the time step sizes are large. Convergence and energy dissipation of the proposed DRLM schemes are confirmed via a manufactured convergence test and the Taylor-Green vortex problem. Additionally, the DRLM schemes accurately capture dynamical evolution in practical scenarios such as the lid-driven cavity flow and Kelvin-Helmholtz instability.

The rest of the paper is organized as follows: In Section 2, we introduce the DRLM formulation for the incompressible NS equations (1.1). The first- and second-order DRLM schemes are derived and shown to be unconditionally energy stable. Fully discrete DRLM schemes with the MAC spatial discretization and their corresponding energy stability are discussed in Section 3. An efficient preconditioning technique is provided in this section to iteratively solve the generalized Stokes systems arising from the fully discrete formulations. In Section 4, we carry out various numerical experiments in 2D and 3D to verify the theoretical findings as well as illustrate the performance of the proposed DRLM schemes with large time-step sizes for long-term simulations. Finally, some concluding remarks are given in Section 5.

2. The DRLM formulation and time-discrete schemes

For any two functions $\boldsymbol{u}, \boldsymbol{v} \in (L^2(\Omega))^d$, denote by $(\boldsymbol{u}, \boldsymbol{v})$ the standard L^2 inner product of $\boldsymbol{u}$ and $\boldsymbol{v}$ on Ω, and $\|\boldsymbol{u}\| = \sqrt{(\boldsymbol{u}, \boldsymbol{u})}$ is the corresponding L^2 norm of $\boldsymbol{u}$. Let $\mathcal{K}(\boldsymbol{u}) = \frac{1}{2}\int_\Omega |\boldsymbol{u}|^2 d\boldsymbol{x}$ be the kinetic energy associated with (1.1), it is clear that

$$\frac{d\mathcal{K}(\boldsymbol{u})}{dt} = (\boldsymbol{u}_t, \boldsymbol{u}) \quad \text{and} \quad (\boldsymbol{F}(\boldsymbol{u}), \boldsymbol{u}) = 0. \tag{2.1}$$

In [44], a Lagrange multiplier $q(t)$ was introduced to reformulate the NS equations (1.1) as follows:

$$\begin{cases} \boldsymbol{u}_t - \nu\Delta\boldsymbol{u} + q\boldsymbol{F}(\boldsymbol{u}) + \nabla p = \boldsymbol{f}, & (2.2a) \\ \nabla\cdot\boldsymbol{u} = 0, & (2.2b) \\ \dfrac{d\mathcal{K}(\boldsymbol{u})}{dt} = (\boldsymbol{u}_t + q\boldsymbol{F}(\boldsymbol{u}), \boldsymbol{u}). & (2.2c) \end{cases}$$

However, the system (2.2) is not equivalent to the original system (1.1) because any constant function $q(t)$ satisfies (2.2c). To ensure the uniqueness of q, we introduce a dynamic term for q in (2.2c) and consider instead the following equations:

$$\begin{cases} \boldsymbol{u}_t - \nu\Delta\boldsymbol{u} + q\boldsymbol{F}(\boldsymbol{u}) + \nabla p = \boldsymbol{f}, & (2.3a) \\ \nabla\cdot\boldsymbol{u} = 0, & (2.3b) \\ \dfrac{d\mathcal{K}(\boldsymbol{u})}{dt} + \theta\dfrac{dq^2}{dt} = (\boldsymbol{u}_t + q\boldsymbol{F}(\boldsymbol{u}), \boldsymbol{u}), & (2.3c) \end{cases}$$

where $q(0) = 1$ and $\theta > 0$ is a regularization parameter to be thoroughly studied in the numerical experiments (cf. Section 4). From (2.1) and (2.3c), we can verify that at the continuous level, $q(t) = 1$ for all $t > 0$. Consequently, the new system (2.3) is equivalent to the original NS equations (1.1). It should be noted that, unlike the SAV approach, the function q serves as a Lagrange multiplier to enforce dissipation of the original energy. Additionally, the parameter θ is crucial in our formulation to guarantee the uniqueness of the Lagrange multiplier at the discrete level, and thus the numerical solutions. Let us next assume a uniform partition of the time interval $[0, T]$: $0 = t_0 < t_1 < \ldots < t_{N_t} = T$ with the time step size $\tau = T/N_t$ and consider the time discretization of the DRLM system (2.3).

Remark 2.1. *In the case of inhomogeneous Dirichlet boundary conditions where* $\boldsymbol{u}|_{\partial\Omega} = \boldsymbol{u}_b$, (2.3c) *is replaced by*

$$\frac{d\mathcal{K}(\boldsymbol{u})}{dt} + \theta\frac{dq^2}{dt} = (\boldsymbol{u}_t, \boldsymbol{u}) + q\left[(\boldsymbol{F}(\boldsymbol{u}), \boldsymbol{u}) - \frac{1}{2}(\boldsymbol{u}_b\cdot\boldsymbol{n}, |\boldsymbol{u}_b|^2)_{\partial\Omega}\right],$$

where $(\cdot,\cdot)_{\partial\Omega}$ *denotes the* L^2 *inner product on* $\partial\Omega$ *and* $\boldsymbol{n}$ *represents the outward unit normal vector to* $\partial\Omega$.

2.1. The first-order in time DRLM scheme

By applying the first-order BDF (i.e., backward Euler) method to equations (2.3a)-(2.3c) with an explicit treatment of the nonlinear convection term, we obtain the following first-order in time DRLM scheme: for $0 \le n \le N_t - 1$,

$$\begin{cases} \dfrac{\boldsymbol{u}^{n+1} - \boldsymbol{u}^n}{\tau} - \nu\Delta\boldsymbol{u}^{n+1} + q^{n+1}\boldsymbol{F}(\boldsymbol{u}^n) + \nabla p^{n+1} = \boldsymbol{f}^{n+1}, & (2.4a) \\ \nabla\cdot\boldsymbol{u}^{n+1} = 0, & (2.4b) \\ \dfrac{\mathcal{K}(\boldsymbol{u}^{n+1}) - \mathcal{K}(\boldsymbol{u}^n)}{\tau} + \theta\dfrac{(q^{n+1})^2 - (q^n)^2}{\tau} = \left(\dfrac{\boldsymbol{u}^{n+1} - \boldsymbol{u}^n}{\tau} + q^{n+1}\boldsymbol{F}(\boldsymbol{u}^n), \boldsymbol{u}^{n+1}\right), & (2.4c) \end{cases}$$

where $\boldsymbol{u}^{n+1}$ satisfies either the periodic or homogeneous Dirichlet boundary conditions, $\boldsymbol{f}^{n+1} = \boldsymbol{f}(t_{n+1})$ is given, $\boldsymbol{u}^n$ and p^n are approximations of $\boldsymbol{u}(t_n)$ and $p(t_n)$, respectively.

Following [22, 23, 24, 44], an efficient implementation of the first-order DRLM scheme (2.4) can be achieved by decomposing each of the unknown quantities, the velocity $\boldsymbol{u}^{n+1}$ and the pressure p^{n+1}, into two components as follows:

$$\boldsymbol{u}^{n+1} = \boldsymbol{u}_1^{n+1} + q^{n+1}\boldsymbol{u}_2^{n+1}, \tag{2.5}$$

$$p^{n+1} = p_1^{n+1} + q^{n+1}p_2^{n+1}. \tag{2.6}$$

Plugging the above equations into the system (2.4), we arrive at

$$\begin{cases} \dfrac{\boldsymbol{u}_1^{n+1} + q^{n+1}\boldsymbol{u}_2^{n+1} - \boldsymbol{u}^n}{\tau} - \nu\Delta(\boldsymbol{u}_1^{n+1} + q^{n+1}\boldsymbol{u}_2^{n+1}) + q^{n+1}\boldsymbol{F}(\boldsymbol{u}^n) \\ \qquad\qquad + \nabla(p_1^{n+1} + q^{n+1}p_2^{n+1}) = \boldsymbol{f}^{n+1}, & \text{(2.7a)} \\ \nabla\cdot(\boldsymbol{u}_1^{n+1} + q^{n+1}\boldsymbol{u}_2^{n+1}) = 0, & \text{(2.7b)} \\ \dfrac{\mathcal{K}(\boldsymbol{u}_1^{n+1} + q^{n+1}\boldsymbol{u}_2^{n+1}) - \mathcal{K}(\boldsymbol{u}^n)}{\tau} + \theta\dfrac{(q^{n+1})^2 - (q^n)^2}{\tau} \\ \qquad = \left(\dfrac{\boldsymbol{u}_1^{n+1} + q^{n+1}\boldsymbol{u}_2^{n+1} - \boldsymbol{u}^n}{\tau} + q^{n+1}\boldsymbol{F}(\boldsymbol{u}^n), \boldsymbol{u}_1^{n+1} + q^{n+1}\boldsymbol{u}_2^{n+1}\right). & \text{(2.7c)} \end{cases}$$

We then split (2.7a) and (2.7b) into two systems of generalized Stokes equations:

$$\begin{cases} \dfrac{\boldsymbol{u}_1^{n+1} - \boldsymbol{u}^n}{\tau} - \nu\Delta\boldsymbol{u}_1^{n+1} + \nabla p_1^{n+1} = \boldsymbol{f}^{n+1}, & \text{(2.8a)} \\ \nabla\cdot\boldsymbol{u}_1^{n+1} = 0, & \text{(2.8b)} \end{cases}$$

and

$$\begin{cases} \dfrac{\boldsymbol{u}_2^{n+1}}{\tau} - \nu\Delta\boldsymbol{u}_2^{n+1} + \boldsymbol{F}(\boldsymbol{u}^n) + \nabla p_2^{n+1} = 0, & \text{(2.9a)} \\ \nabla\cdot\boldsymbol{u}_2^{n+1} = 0, & \text{(2.9b)} \end{cases}$$

where $\boldsymbol{u}_1^{n+1}$ and $\boldsymbol{u}_2^{n+1}$ satisfy the same boundary conditions as $\boldsymbol{u}^{n+1}$, i.e., either homogeneous Dirichlet or periodic boundary conditions. For the NS equations with inhomogeneous Dirichlet data $\boldsymbol{u}|_{\partial\Omega} = \boldsymbol{u}_b$, we impose $\boldsymbol{u}_1^{n+1} = \boldsymbol{u}_b(t_{n+1})$ and $\boldsymbol{u}_2^{n+1} = 0$ on $\partial\Omega$.

Note that the two systems (2.8) and (2.9) are linear and can be solved independently of q^{n+1} (cf. Subsection 3.3 and [22, 30]). Once $\boldsymbol{u}_1^{n+1}, \boldsymbol{u}_2^{n+1}, p_1^{n+1}$, and p_2^{n+1} are determined, we compute q^{n+1} from (2.7c) by solving the quadratic equation:

$$A_{1,n+1}(q^{n+1})^2 + B_{1,n+1}q^{n+1} + C_{1,n+1} = 0, \tag{2.10}$$

where

$$\begin{aligned} A_{1,n+1} &= \frac{1}{2}\|\boldsymbol{u}_2^{n+1}\|^2 + \theta + \tau\nu\|\nabla\boldsymbol{u}_2^{n+1}\|^2, \\ B_{1,n+1} &= -(\boldsymbol{u}_1^{n+1} - \boldsymbol{u}^n, \boldsymbol{u}_2^{n+1}) - \tau(\boldsymbol{F}(\boldsymbol{u}^n), \boldsymbol{u}_1^{n+1}), \\ C_{1,n+1} &= -\frac{1}{2}\|\boldsymbol{u}_1^{n+1} - \boldsymbol{u}^n\|^2 - \theta(q^n)^2. \end{aligned}$$

To derive $A_{1,n+1}$, we have used the property $(\frac{1}{\tau}\boldsymbol{u}_2^{n+1} + \boldsymbol{F}(\boldsymbol{u}^n), \boldsymbol{u}_2^{n+1}) = -\nu\|\nabla\boldsymbol{u}_2^{n+1}\|^2$ obtained from (2.9) and integration by parts.

We remark that $A_{1,n+1} > 0$ and $C_{1,n+1} < 0$ for any $\theta > 0$. Therefore, the quadratic equation (2.10) has a *unique positive solution* q^{n+1} for any positive regularization parameter θ. Once q^{n+1} is known, we update $\boldsymbol{u}^{n+1}$ and p^{n+1} using equations (2.5) and (2.6), respectively.

2.2. The second-order in time DRLM scheme

To construct the second-order DRLM scheme, we assume $\boldsymbol{u}^{n-1}$ and $\boldsymbol{u}^n$ are given and denote by $\tilde{\boldsymbol{u}}^{n+1} = 2\boldsymbol{u}^n - \boldsymbol{u}^{n-1}$ the second-order extrapolation to be used for the approximation of the nonlinear convection term. By applying the BDF2 method to equations (2.3a)-(2.3c), we obtain the following second-order DRLM scheme: for $1 \le n \le N_t - 1$,

$$\begin{cases} \dfrac{3\boldsymbol{u}^{n+1} - 4\boldsymbol{u}^n + \boldsymbol{u}^{n-1}}{2\tau} - \nu\Delta\boldsymbol{u}^{n+1} + q^{n+1}\boldsymbol{F}(\tilde{\boldsymbol{u}}^{n+1}) + \nabla p^{n+1} = \boldsymbol{f}^{n+1}, & \text{(2.11a)} \\ \nabla\cdot\boldsymbol{u}^{n+1} = 0, & \text{(2.11b)} \\ \dfrac{3\mathcal{K}(\boldsymbol{u}^{n+1}) - 4\mathcal{K}(\boldsymbol{u}^n) + \mathcal{K}(\boldsymbol{u}^{n-1})}{2\tau} + \theta\dfrac{3(q^{n+1})^2 - 4(q^n)^2 + (q^{n-1})^2}{2\tau} \\ \qquad = \left(\dfrac{3\boldsymbol{u}^{n+1} - 4\boldsymbol{u}^n + \boldsymbol{u}^{n-1}}{2\tau} + q^{n+1}\boldsymbol{F}(\tilde{\boldsymbol{u}}^{n+1}), \boldsymbol{u}^{n+1}\right), & \text{(2.11c)} \end{cases}$$

where $\boldsymbol{u}^{n+1}$ satisfies either the periodic or homogeneous Dirichlet boundary conditions, $\boldsymbol{u}^1$ and q^1 are computed using the first-order DRLM scheme (2.4).

The second-order DRLM scheme (2.11) can also be implemented efficiently by again decomposing each of the two unknowns $\boldsymbol{u}^{n+1}$ and p^{n+1} into two components, as in (2.5) and (2.6). From (2.11a) and (2.11b), we obtain the generalized Stokes systems for $\boldsymbol{u}_i^{n+1}$ and p_i^{n+1} $(i = 1, 2)$ as follows:

$$\begin{cases} \dfrac{3\boldsymbol{u}_1^{n+1} - 4\boldsymbol{u}^n + \boldsymbol{u}^{n-1}}{2\tau} - \nu\Delta\boldsymbol{u}_1^{n+1} + \nabla p_1^{n+1} = \boldsymbol{f}^{n+1}, & \text{(2.12a)} \\ \nabla\cdot\boldsymbol{u}_1^{n+1} = 0, & \text{(2.12b)} \end{cases}$$

and

$$\begin{cases} \dfrac{3\boldsymbol{u}_2^{n+1}}{2\tau} - \nu\Delta\boldsymbol{u}_2^{n+1} + \boldsymbol{F}(\tilde{\boldsymbol{u}}^{n+1}) + \nabla p_2^{n+1} = 0, & \text{(2.13a)} \\ \nabla\cdot\boldsymbol{u}_2^{n+1} = 0. & \text{(2.13b)} \end{cases}$$

After determining $\boldsymbol{u}_i^{n+1}$ and p_i^{n+1} $(i = 1, 2)$ from the linear systems (2.12) and (2.13), the discrete Lagrange multiplier q^{n+1} is obtained from (2.11c) by solving the quadratic equation:

$$A_{2,n+1}(q^{n+1})^2 + B_{2,n+1}q^{n+1} + C_{2,n+1} = 0, \tag{2.14}$$

where

$$\begin{aligned} A_{2,n+1} &= \frac{3}{2}\|\boldsymbol{u}_2^{n+1}\|^2 + 3\theta + 2\tau\nu\|\nabla\boldsymbol{u}_2^{n+1}\|^2, \\ B_{2,n+1} &= -(3\boldsymbol{u}_1^{n+1} - 4\boldsymbol{u}^n + \boldsymbol{u}^{n-1}, \boldsymbol{u}_2^{n+1}) - 2\tau(\boldsymbol{F}(\tilde{\boldsymbol{u}}^{n+1}), \boldsymbol{u}_1^{n+1}), \\ C_{2,n+1} &= -2\|\boldsymbol{u}_1^{n+1} - \boldsymbol{u}^n\|^2 + \frac{1}{2}\|\boldsymbol{u}_1^{n+1} - \boldsymbol{u}^{n-1}\|^2 - \theta\left[4(q^n)^2 - (q^{n-1})^2\right]. \end{aligned}$$

To derive $A_{2,n+1}$, we have used the fact that $(\frac{3}{2\tau}\boldsymbol{u}_2^{n+1} + \boldsymbol{F}(\tilde{\boldsymbol{u}}^{n+1}), \boldsymbol{u}_2^{n+1}) = -\nu\|\nabla\boldsymbol{u}_2^{n+1}\|^2$ due to (2.13) and integration by parts. Since $A_{2,n+1} > 0$ for all $\theta > 0$, the algebraic equation (2.14) attains two solutions:

$$q_{\pm}^{n+1} = \frac{-B_{2,n+1} \pm \sqrt{B_{2,n+1}^2 - 4A_{2,n+1}C_{2,n+1}}}{2A_{2,n+1}}.$$

Because the exact value of q is 1, we choose the root that is closer to 1. We observe numerically that $C_{2,n+1} < 0$ if θ is sufficiently large, making $q^{n+1} = q_+^{n+1}$ the unique positive solution. Finally, $\boldsymbol{u}^{n+1}$ and p^{n+1} are computed from (2.5) and (2.6), respectively.

Remark 2.2. *Another possible way to construct the DRLM scheme of order 2 is based on the Crank-Nicolson method, where the time-discrete version of* (2.3) *is given by*

$$\begin{cases} \dfrac{\boldsymbol{u}^{n+1}-\boldsymbol{u}^n}{\tau} - \nu\Delta\boldsymbol{u}^{n+1/2} + q^{n+1/2}\boldsymbol{F}(\tilde{\boldsymbol{u}}^{n+1/2}) + \nabla p^{n+1/2} = \boldsymbol{f}^{n+1/2}, & \text{(2.15a)} \\ \nabla\cdot\boldsymbol{u}^{n+1/2} = 0, & \text{(2.15b)} \\ \dfrac{\mathcal{K}(\boldsymbol{u}^{n+1})-\mathcal{K}(\boldsymbol{u}^n)}{\tau} + \theta\dfrac{(q^{n+1})^2-(q^n)^2}{\tau} = \left(\dfrac{\boldsymbol{u}^{n+1}-\boldsymbol{u}^n}{\tau} + q^{n+1/2}\boldsymbol{F}(\tilde{\boldsymbol{u}}^{n+1/2}), \boldsymbol{u}^{n+1/2}\right), & \text{(2.15c)} \end{cases}$$

where $\boldsymbol{f}^{n+1/2} = \boldsymbol{f}(t_{n+1/2})$, $\tilde{\boldsymbol{u}}^{n+1/2} = \frac{1}{2}(3\boldsymbol{u}^n - \boldsymbol{u}^{n-1})$, *and* $\psi^{n+1/2} = \frac{1}{2}(\psi^n + \psi^{n+1})$ *for* $\psi \in \{\boldsymbol{u}, p, q\}$. *Note that* $\tilde{\boldsymbol{u}}^{1/2}$ *can be computed by the following first-order scheme [22]:*

$$\frac{\tilde{\boldsymbol{u}}^{1/2}-\boldsymbol{u}^0}{\tau/2} - \nu\Delta\tilde{\boldsymbol{u}}^{1/2} + \boldsymbol{F}(\boldsymbol{u}^0) + \nabla\tilde{p}^{1/2} = \boldsymbol{f}^{1/2}, \quad \nabla\cdot\tilde{\boldsymbol{u}}^{1/2} = 0,$$

which has a local truncation error of $\mathcal{O}(\tau^2)$. *We remark that all the terms involving the kinetic energy in* (2.15c) *disappear after simplification. Indeed, by the definition of* $\mathcal{K}(\boldsymbol{u})$ *we have:*

$$\frac{\mathcal{K}(\boldsymbol{u}^{n+1})-\mathcal{K}(\boldsymbol{u}^n)}{\tau} = \frac{1}{2\tau}\left[(\boldsymbol{u}^{n+1},\boldsymbol{u}^{n+1}) - (\boldsymbol{u}^n,\boldsymbol{u}^n)\right] = \left(\frac{\boldsymbol{u}^{n+1}-\boldsymbol{u}^n}{\tau}, \boldsymbol{u}^{n+1/2}\right).$$

Therefore, (2.15c) *is reduced to* $\theta\frac{(q^{n+1})^2-(q^n)^2}{\tau} = \left(q^{n+1/2}\boldsymbol{F}(\tilde{\boldsymbol{u}}^{n+1/2}), \boldsymbol{u}^{n+1/2}\right)$, *or equivalently (note that* $q^{n+1}+q^n = 2q^{n+1/2} \neq 0$*),*

$$\theta\frac{q^{n+1}-q^n}{\tau} = \frac{1}{2}\left(\boldsymbol{F}(\tilde{\boldsymbol{u}}^{n+1/2}), \boldsymbol{u}^{n+1/2}\right). \tag{2.16}$$

From this equation q^{n+1} *is uniquely determined. Note that* (2.16) *is equivalent to the Crank-Nicolson discretization of equation* $\theta\frac{dq}{dt} = \frac{1}{2}(\boldsymbol{F}(\boldsymbol{u}), \boldsymbol{u})$.

Remark 2.3. *The proposed DRLM schemes involve solving two systems of generalized Stokes equations at each time step. Alternatively, one can replace the Stokes solver with two Poisson solvers via the pressure-correction approach; we refer to [12, 13, 23, 25, 44] for a detailed discussion of this approach in the context of the NS equations, and [4, 26, 37] for other incompressible fluid models. To that end, a pressure-correction variant of the first-order DRLM scheme* (2.4) *is given by*

$$\begin{cases} \dfrac{\overline{\boldsymbol{u}}^{n+1}-\boldsymbol{u}^n}{\tau} - \nu\Delta\overline{\boldsymbol{u}}^{n+1} + q^{n+1}\boldsymbol{F}(\boldsymbol{u}^n) + \nabla p^n = \boldsymbol{f}^{n+1}, & \text{(2.17a)} \\ \dfrac{\boldsymbol{u}^{n+1}-\overline{\boldsymbol{u}}^{n+1}}{\tau} + \nabla(p^{n+1}-p^n) = \boldsymbol{0}, & \text{(2.17b)} \\ \nabla\cdot\boldsymbol{u}^{n+1} = 0, & \text{(2.17c)} \\ \dfrac{\mathcal{K}(\boldsymbol{u}^{n+1})-\mathcal{K}(\boldsymbol{u}^n)}{\tau} + \theta\dfrac{(q^{n+1})^2-(q^n)^2}{\tau} = \left(\dfrac{\boldsymbol{u}^{n+1}-\boldsymbol{u}^n}{\tau} + q^{n+1}\boldsymbol{F}(\boldsymbol{u}^n), \overline{\boldsymbol{u}}^{n+1}\right), & \text{(2.17d)} \end{cases}$$

and a rotational pressure-correction variant of the second-order DRLM scheme (2.11) *by*

$$\begin{cases} \dfrac{3\overline{\boldsymbol{u}}^{n+1}-4\boldsymbol{u}^{n}+\boldsymbol{u}^{n-1}}{2\tau}-\nu\Delta\overline{\boldsymbol{u}}^{n+1}+q^{n+1}\boldsymbol{F}(\tilde{\boldsymbol{u}}^{n+1})+\nabla p^{n}=\boldsymbol{f}^{n+1}, & \text{(2.18a)}\\ \dfrac{3\boldsymbol{u}^{n+1}-3\overline{\boldsymbol{u}}^{n+1}}{2\tau}+\nabla(p^{n+1}-p^{n}+\nu\nabla\cdot\overline{\boldsymbol{u}}^{n+1})=\boldsymbol{0}, & \text{(2.18b)}\\ \nabla\cdot\boldsymbol{u}^{n+1}=0, & \text{(2.18c)}\\ \dfrac{3\mathcal{K}(\boldsymbol{u}^{n+1})-4\mathcal{K}(\boldsymbol{u}^{n})+\mathcal{K}(\boldsymbol{u}^{n-1})}{2\tau}+\theta\dfrac{3(q^{n+1})^2-4(q^{n})^2+(q^{n-1})^2}{2\tau} & \\ \qquad=\left(\dfrac{3\boldsymbol{u}^{n+1}-4\boldsymbol{u}^{n}+\boldsymbol{u}^{n-1}}{2\tau}+q^{n+1}\boldsymbol{F}(\tilde{\boldsymbol{u}}^{n+1}),\overline{\boldsymbol{u}}^{n+1}\right), & \text{(2.18d)} \end{cases}$$

where $\overline{\boldsymbol{u}}^{n+1}$ *and* $\boldsymbol{u}^{n+1}$ *in* (2.17) *and* (2.18) *satisfy the periodic boundary conditions or* $\overline{\boldsymbol{u}}^{n+1}|_{\partial\Omega}=0$ *and* $\boldsymbol{u}^{n+1}\cdot\boldsymbol{n}|_{\partial\Omega}=0$. *Note that we have used the rotational form in* (2.18) *since the standard second-order pressure-correction approach may limit the accuracy of the scheme due to certain artificial boundary conditions, as discussed in [12, 13]. The stability of the pressure-correction DRLM schemes* (2.17) *and* (2.18) *will be discussed in Remark 2.6.*

2.3. Time-discrete energy stability

In this subsection, we aim to establish energy stability of the proposed first- and second-order DRLM schemes.

Theorem 2.1. *In the absence of the external force* $\boldsymbol{f}$*, the first-order DRLM scheme* (2.4) *is unconditionally stable in the sense that*

$$\mathcal{K}(\boldsymbol{u}^{n+1})+\theta[(q^{n+1})^2-1]\le\mathcal{K}(\boldsymbol{u}^{n})+\theta[(q^{n})^2-1],\quad n=0,1,\cdots,N_t-1.$$

Proof. Taking the L^2 inner product on both sides of (2.4a) with $\boldsymbol{u}^{n+1}$, we have

$$\left(\frac{\boldsymbol{u}^{n+1}-\boldsymbol{u}^{n}}{\tau}+q^{n+1}\boldsymbol{F}(\boldsymbol{u}^{n}),\boldsymbol{u}^{n+1}\right)=(\nu\Delta\boldsymbol{u}^{n+1}-\nabla p^{n+1},\boldsymbol{u}^{n+1})=-\nu\|\nabla\boldsymbol{u}^{n+1}\|^2, \tag{2.19}$$

where we used the fact that $(\nabla p^{n+1},\boldsymbol{u}^{n+1})=0$ due to the divergence-free condition (2.4b), boundary conditions of $\boldsymbol{u}^{n+1}$, and integration by parts. The combination of (2.4c) and (2.19) yields

$$\frac{\mathcal{K}(\boldsymbol{u}^{n+1})-\mathcal{K}(\boldsymbol{u}^{n})}{\tau}+\theta\frac{(q^{n+1})^2-(q^{n})^2}{\tau}=-\nu\|\nabla\boldsymbol{u}^{n+1}\|^2\le 0.$$

This implies that

$$\mathcal{K}(\boldsymbol{u}^{n+1})+\theta(q^{n+1})^2\le\mathcal{K}(\boldsymbol{u}^{n})+\theta(q^{n})^2,$$

which completes the proof of Theorem 2.1. □

Remark 2.4. *We have from Theorem 2.1 that*

$$0\le\mathcal{K}(\boldsymbol{u}^{n})+\theta(q^{n})^2\le\mathcal{K}(\boldsymbol{u}^{n-1})+\theta(q^{n-1})^2\le\ldots\le\mathcal{K}(\boldsymbol{u}^{0})+\theta(q^{0})^2=\mathcal{K}(\boldsymbol{u}^{0})+\theta.$$

Thus, the discrete energy $\{\mathcal{K}(\boldsymbol{u}^{n})\}_{n=0}^{N_t}$ *is uniformly bounded for the first-order scheme* (2.4).

Theorem 2.2. *In the absence of the external force $\boldsymbol{f}$, the second-order DRLM scheme* (2.11) *is unconditionally stable in the sense that*

$$\begin{aligned}\frac{3}{2}\mathcal{K}(\boldsymbol{u}^{n+1})-\frac{1}{2}\mathcal{K}(\boldsymbol{u}^{n})+\theta\left[\frac{3}{2}(q^{n+1})^2-\frac{1}{2}(q^{n})^2-1\right]\\ \leq \frac{3}{2}\mathcal{K}(\boldsymbol{u}^{n})-\frac{1}{2}\mathcal{K}(\boldsymbol{u}^{n-1})+\theta\left[\frac{3}{2}(q^{n})^2-\frac{1}{2}(q^{n-1})^2-1\right],\quad n=1,2,\cdots,N_t-1. \quad (2.20)\end{aligned}$$

Proof. Multiplying both sides of equation (2.11a) with $\boldsymbol{u}^{n+1}$ and using (2.11b), we find that

$$\begin{aligned}\left(\frac{3\boldsymbol{u}^{n+1}-4\boldsymbol{u}^{n}+\boldsymbol{u}^{n-1}}{2\tau}+q^{n+1}\boldsymbol{F}(\tilde{\boldsymbol{u}}^{n+1}),\boldsymbol{u}^{n+1}\right)&=(\nu\Delta\boldsymbol{u}^{n+1}-\nabla p^{n+1},\boldsymbol{u}^{n+1})\\ &=-\nu\|\nabla\boldsymbol{u}^{n+1}\|^2\leq 0.\end{aligned}$$

This, together with (2.11c), gives us

$$\frac{3\mathcal{K}(\boldsymbol{u}^{n+1})-4\mathcal{K}(\boldsymbol{u}^{n})+\mathcal{K}(\boldsymbol{u}^{n-1})}{2\tau}+\theta\frac{3(q^{n+1})^2-4(q^{n})^2+(q^{n-1})^2}{2\tau}\leq 0,$$

or equivalently,

$$3\mathcal{K}(\boldsymbol{u}^{n+1})-\mathcal{K}(\boldsymbol{u}^{n})+\theta\left[3(q^{n+1})^2-(q^{n})^2\right]\leq 3\mathcal{K}(\boldsymbol{u}^{n})-\mathcal{K}(\boldsymbol{u}^{n-1})+\theta\left[3(q^{n})^2-(q^{n-1})^2\right].$$

Thus, we obtain the desired estimate. □

Remark 2.5. *(i) We note that* (2.20) *is equivalent to the following estimate*

$$\mathcal{K}(\tilde{\boldsymbol{u}}^{n+3/2})+\theta[(\tilde{q}^{n+3/2})^2-1]\leq\mathcal{K}(\tilde{\boldsymbol{u}}^{n+1/2})+\theta[(\tilde{q}^{n+1/2})^2-1]+\varepsilon^{n+1},$$

where $\tilde{\boldsymbol{u}}^{n+1/2}=\frac{1}{2}(3\boldsymbol{u}^{n}-\boldsymbol{u}^{n-1})$ and $\tilde{q}^{n+1/2}=\frac{1}{2}(3q^{n}-q^{n-1})$ for $n\geq 1$ are second-order approximations of $\boldsymbol{u}(t_{n+1/2})$ and $q(t_{n+1/2})$, respectively, and

$$\varepsilon^{n+1}=\frac{3}{4}\left[\mathcal{K}(\boldsymbol{u}^{n+1}-\boldsymbol{u}^{n})-\mathcal{K}(\boldsymbol{u}^{n}-\boldsymbol{u}^{n-1})+\theta(q^{n+1}-q^{n})^2-\theta(q^{n}-q^{n-1})^2\right].$$

Therefore, if $\|\boldsymbol{u}^{n+1}-\boldsymbol{u}^{n}\|\leq c\tau$ and $|q^{n+1}-q^{n}|\leq c\tau$ for all $n\geq 0$, then $\varepsilon^{n+1}=\mathcal{O}(\tau^2)$.

(ii) It follows from Theorem 2.2 that

$$\frac{3}{2}\mathcal{K}(\boldsymbol{u}^{n+1})+\frac{3}{2}\theta(q^{n+1})^2\leq\frac{1}{2}\mathcal{K}(\boldsymbol{u}^{n})+\frac{1}{2}\theta(q^{n})^2+C, \quad (2.21)$$

where $C=\frac{3}{2}\mathcal{K}(\boldsymbol{u}^{1})-\frac{1}{2}\mathcal{K}(\boldsymbol{u}^{0})+\theta\left[\frac{3}{2}(q^{1})^2-\frac{1}{2}(q^{0})^2\right]$. By repeatedly applying (2.21), *we deduce that*

$$\mathcal{K}(\boldsymbol{u}^{n})+\theta(q^{n})^2\leq\frac{1}{3^n}\left(\mathcal{K}(\boldsymbol{u}^{0})+\theta(q^{0})^2-C\right)+C,$$

which indicates the boundedness of the energy functional for the second-order scheme (2.11).

(iii) By using similar arguments as in the proofs of Theorems 2.1 and 2.2, we can show that the second-order DRLM scheme based on the Crank-Nicolson method (2.15) *is unconditionally stable in the sense that*

$$\mathcal{K}(\boldsymbol{u}^{n+1})+\theta[(q^{n+1})^2-1]\leq\mathcal{K}(\boldsymbol{u}^{n})+\theta[(q^{n})^2-1],\quad n=0,1,\cdots,N_t-1.$$

Note that the energy stability result is improved with the Crank-Nicolson scheme, compared to the BDF2 method (cf. (2.20)*). However, for dissipative systems, the second-order BDF method usually has better numerical performance than the Crank-Nicolson counterpart [6]. Therefore, in the following sections, we focus on the DRLM schemes based on the first- and second-order BDF methods.*

Remark 2.6. *For the pressure-correction versions of the proposed DRLM schemes, the following energy stability results hold (assuming* $\boldsymbol{f} = \mathbf{0}$*):*

$$\mathcal{K}(\boldsymbol{u}^{n+1}) + \frac{\tau^2}{2}\|\nabla p^{n+1}\|^2 + \theta[(q^{n+1})^2 - 1] \le \mathcal{K}(\boldsymbol{u}^n) + \frac{\tau^2}{2}\|\nabla p^n\|^2 + \theta[(q^n)^2 - 1], \tag{2.22}$$

for the first-order pressure-correction DRLM scheme (2.17)*, and*

$$\begin{aligned}&\frac{3}{2}\mathcal{K}(\boldsymbol{u}^{n+1}) - \frac{1}{2}\mathcal{K}(\boldsymbol{u}^n) + \frac{\tau^2}{3}\|\nabla(p^{n+1} + \nu s^{n+1})\|^2 + \frac{\tau\nu}{2}\|s^{n+1}\|^2 + \theta\left[\frac{3}{2}(q^{n+1})^2 - \frac{1}{2}(q^n)^2 - 1\right]\\ &\quad\le \frac{3}{2}\mathcal{K}(\boldsymbol{u}^n) - \frac{1}{2}\mathcal{K}(\boldsymbol{u}^{n-1}) + \frac{\tau^2}{3}\|\nabla(p^n + \nu s^n)\|^2 + \frac{\tau\nu}{2}\|s^n\|^2 + \theta\left[\frac{3}{2}(q^n)^2 - \frac{1}{2}(q^{n-1})^2 - 1\right],\end{aligned} \tag{2.23}$$

for the second-order rotational pressure-correction DRLM scheme (2.18)*, where* $s^n := \nabla \cdot \sum_{i=1}^{n} \overline{\boldsymbol{u}}^i$ *for* $1 \le n \le N_t$*. Detailed proofs of these estimates are provided in Appendix A and Appendix B, respectively.*

3. Fully discrete DRLM schemes

In this section, we apply spatial discretization for the time-discrete problems (2.4) and (2.11) to obtain fully discrete DRLM schemes. While the proposed DRLM approach can be coupled with finite difference, finite element, or finite volume methods, we adopt the finite difference approximation on a MAC staggered grid for simplicity. The corresponding energy stability of the numerical solutions is then rigorously established. The proposed schemes require solving two generalized Stokes systems and a quadratic equation at each time step, with the former being the main computational cost, especially for large Reynolds numbers. Therefore, we discuss preconditioned iterative solvers for Stokes systems at the end of the section.

3.1. The MAC scheme for spatial discretization

To simplify the presentation, we consider the 2D NS equations (1.1) with the spatial domain $\Omega = (0,1)^2$, the external force $\boldsymbol{f} = [f_1, f_2]^T$, and the velocity vector field $\boldsymbol{u} = [u, v]^T$. The extension to the 3D case can be done in a similar manner. Suppose that Ω is partitioned into $N_x N_y$ rectangles of the form $(x_{i-1}, x_i) \times (y_{j-1}, y_j)$ for $1 \le i \le N_x$ and $1 \le j \le N_y$, where

$$0 = x_0 < x_1 < \ldots < x_{N_x} = 1, \quad \text{and} \quad 0 = y_0 < y_1 < \ldots < y_{N_y} = 1.$$

Let $h_x = \frac{1}{N_x}$ and $h_y = \frac{1}{N_y}$ be the uniform mesh sizes in the x- and y-directions, respectively. For $\psi \in \{u, v, p\}$, let $\Omega_{h,\psi}$ represent the collection of discrete points in Ω associated with ψ (see Figure 1);

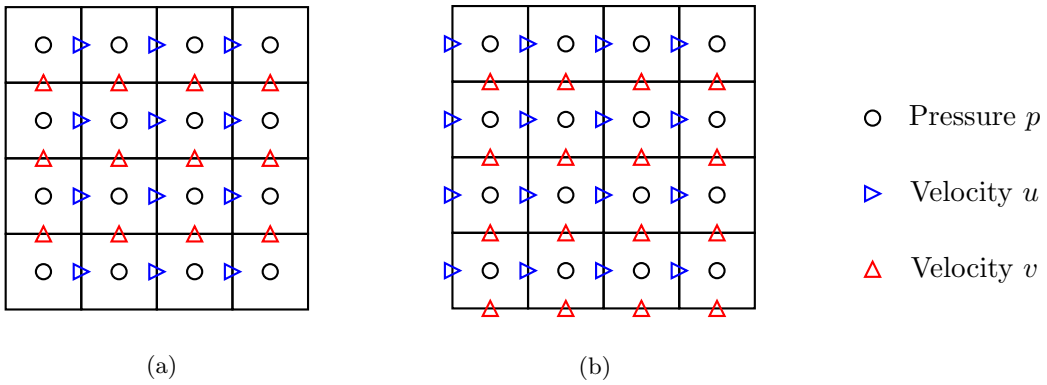

Figure 1: Staggered grid ($N_x = N_y = 4$) for spatial discretization with positions of unknowns u, v, and p. (a) Homogeneous Dirichlet boundary conditions. (b) Periodic boundary conditions.

in particular, $\Omega_{h,p}$ corresponds to black circle points, $\Omega_{h,u}$ to blue right-pointing triangles, and $\Omega_{h,v}$ to red upward-pointing triangles. Denote by $\boldsymbol{U}^n, \boldsymbol{V}^n$, and $\boldsymbol{P}^n$ $(0 \le n \le N_t)$ the approximations of u^n, v^n, and p^n over $\Omega_{h,u}, \Omega_{h,v}$, and $\Omega_{h,p}$, respectively. For any two matrices $\boldsymbol{A}$ and $\boldsymbol{B}$ of the same size, we define

$$(\boldsymbol{A}, \boldsymbol{B})_{l^2} := h_x h_y \mathrm{Tr}(\boldsymbol{A}^T \boldsymbol{B}), \qquad \|\boldsymbol{A}\|_{l^2} := \sqrt{(\boldsymbol{A}, \boldsymbol{A})_{l^2}},$$

as the discrete l^2 inner product and corresponding l^2 norm.

Next, we introduce differentiation matrices for Δu, Δv, and ∇p, utilizing the following matrices for any positive integer N and real numbers h and a:

$$\boldsymbol{K}^{\mathrm{Dir}}_{N,h,a} = \frac{1}{h^2}\begin{bmatrix} -a & 1 & 0 & \dots & 0 \\ 1 & -2 & 1 & \dots & 0 \\ \vdots & \ddots & \ddots & \ddots & \vdots \\ 0 & \dots & 1 & -2 & 1 \\ 0 & \dots & 0 & 1 & -a \end{bmatrix}_{N\times N} \qquad \boldsymbol{M}^{\mathrm{Dir}}_{N,h} = \frac{1}{h}\begin{bmatrix} -1 & 1 & 0 & \dots & 0 \\ 0 & -1 & 1 & \dots & 0 \\ \vdots & \ddots & \ddots & \ddots & \vdots \\ 0 & \dots & 0 & -1 & 1 \end{bmatrix}_{(N-1)\times N},$$

$$\boldsymbol{K}^{\mathrm{per}}_{N,h} = \frac{1}{h^2}\begin{bmatrix} -2 & 1 & 0 & \dots & 1 \\ 1 & -2 & 1 & \dots & 0 \\ \vdots & \ddots & \ddots & \ddots & \vdots \\ 0 & \dots & 1 & -2 & 1 \\ 1 & \dots & 0 & 1 & -2 \end{bmatrix}_{N\times N} \qquad \boldsymbol{M}^{\mathrm{per}}_{N,h} = \frac{1}{h}\begin{bmatrix} 1 & 0 & 0 & \dots & -1 \\ -1 & 1 & 0 & \dots & 0 \\ \vdots & \ddots & \ddots & \ddots & \vdots \\ 0 & \dots & -1 & 1 & 0 \\ 0 & \dots & 0 & -1 & 1 \end{bmatrix}_{N\times N}.$$

For homogeneous Dirichlet boundary conditions, we define the matrices $\boldsymbol{A}_u$, $\boldsymbol{B}_u$, $\boldsymbol{A}_v$, $\boldsymbol{B}_v$, $\boldsymbol{A}_p$, and $\boldsymbol{B}_p$ as follows:

$$\boldsymbol{A}_u = \boldsymbol{K}^{\mathrm{Dir}}_{N_x-1,h_x,2}, \qquad \boldsymbol{A}_v = \boldsymbol{K}^{\mathrm{Dir}}_{N_x,h_x,3}, \qquad \boldsymbol{A}_p = \boldsymbol{M}^{\mathrm{Dir}}_{N_x,h_x}, \tag{3.1}$$

$$\boldsymbol{B}_u = \boldsymbol{K}^{\mathrm{Dir}}_{N_y,h_y,3}, \qquad \boldsymbol{B}_v = \boldsymbol{K}^{\mathrm{Dir}}_{N_y-1,h_y,2}, \qquad \boldsymbol{B}_p = \boldsymbol{M}^{\mathrm{Dir}}_{N_y,h_y}. \tag{3.2}$$

For periodic boundary conditions, we set

$$\boldsymbol{A}_u = \boldsymbol{A}_v = \boldsymbol{K}^{\mathrm{per}}_{N_x,h_x}, \qquad \boldsymbol{A}_p = \boldsymbol{M}^{\mathrm{per}}_{N_x,h_x}, \tag{3.3}$$

$$\boldsymbol{B}_u = \boldsymbol{B}_v = \boldsymbol{K}^{\mathrm{per}}_{N_y,h_y}, \qquad \boldsymbol{B}_p = \boldsymbol{M}^{\mathrm{per}}_{N_y,h_y}. \tag{3.4}$$

Applying the central finite difference method on the staggered grid (cf. Figure 1) to system (2.4) results in the fully discrete first-order DRLM scheme:

$$\begin{cases} \dfrac{\boldsymbol{U}^{n+1}-\boldsymbol{U}^n}{\tau} - \nu\left(\boldsymbol{A}_u\boldsymbol{U}^{n+1} + \boldsymbol{U}^{n+1}\boldsymbol{B}_u^T\right) + q^{n+1}\boldsymbol{F}_1(\boldsymbol{U}^n,\boldsymbol{V}^n) + \boldsymbol{A}_p\boldsymbol{P}^{n+1} = \mathcal{F}_1^{n+1}, & (3.5a)\\ \dfrac{\boldsymbol{V}^{n+1}-\boldsymbol{V}^n}{\tau} - \nu\left(\boldsymbol{A}_v\boldsymbol{V}^{n+1} + \boldsymbol{V}^{n+1}\boldsymbol{B}_v^T\right) + q^{n+1}\boldsymbol{F}_2(\boldsymbol{U}^n,\boldsymbol{V}^n) + \boldsymbol{P}^{n+1}\boldsymbol{B}_p^T = \mathcal{F}_2^{n+1}, & (3.5b)\\ (-\boldsymbol{A}_p^T)\boldsymbol{U}^{n+1} + \boldsymbol{V}^{n+1}(-\boldsymbol{B}_p) = \boldsymbol{O}, & (3.5c)\\ \dfrac{1}{2\tau}\left(\|\boldsymbol{U}^{n+1}\|_{l^2}^2 + \|\boldsymbol{V}^{n+1}\|_{l^2}^2 - \|\boldsymbol{U}^n\|_{l^2}^2 - \|\boldsymbol{V}^n\|_{l^2}^2\right) + \theta\dfrac{(q^{n+1})^2-(q^n)^2}{\tau} \\ = \left(\dfrac{\boldsymbol{U}^{n+1}-\boldsymbol{U}^n}{\tau} + q^{n+1}\boldsymbol{F}_1(\boldsymbol{U}^n,\boldsymbol{V}^n),\boldsymbol{U}^{n+1}\right)_{l^2} + \left(\dfrac{\boldsymbol{V}^{n+1}-\boldsymbol{V}^n}{\tau} + q^{n+1}\boldsymbol{F}_2(\boldsymbol{U}^n,\boldsymbol{V}^n),\boldsymbol{V}^{n+1}\right)_{l^2}. & (3.5d) \end{cases}$$

Here, $\mathcal{F}_1$ and $\mathcal{F}_2$ represent the discrete evaluations of f_1 and f_2 over $\Omega_{h,u}$ and $\Omega_{h,v}$, respectively. Similarly, $\boldsymbol{F}_1(\boldsymbol{U},\boldsymbol{V})$ and $\boldsymbol{F}_2(\boldsymbol{U},\boldsymbol{V})$ approximate the nonlinear convection terms $uu_x + vu_y$ and $uv_x + vv_y$ on the grids $\Omega_{h,u}$ and $\Omega_{h,v}$, respectively.

For the second-order case (2.11), we define $\tilde{\boldsymbol{U}}^{n+1} = 2\boldsymbol{U}^n - \boldsymbol{U}^{n-1}$ and $\tilde{\boldsymbol{V}}^{n+1} = 2\boldsymbol{V}^n - \boldsymbol{V}^{n-1}$ for $n \geq 1$. The fully discrete second-order DRLM scheme is given by:

$$\begin{cases} \dfrac{3\boldsymbol{U}^{n+1}-4\boldsymbol{U}^n+\boldsymbol{U}^{n-1}}{2\tau} - \nu\left(\boldsymbol{A}_u\boldsymbol{U}^{n+1} + \boldsymbol{U}^{n+1}\boldsymbol{B}_u^T\right) + q^{n+1}\boldsymbol{F}_1(\tilde{\boldsymbol{U}}^{n+1},\tilde{\boldsymbol{V}}^{n+1}) + \boldsymbol{A}_p\boldsymbol{P}^{n+1} = \mathcal{F}_1^{n+1}, & (3.6a)\\ \dfrac{3\boldsymbol{V}^{n+1}-4\boldsymbol{V}^n+\boldsymbol{V}^{n-1}}{2\tau} - \nu\left(\boldsymbol{A}_v\boldsymbol{V}^{n+1} + \boldsymbol{V}^{n+1}\boldsymbol{B}_v^T\right) + q^{n+1}\boldsymbol{F}_2(\tilde{\boldsymbol{U}}^{n+1},\tilde{\boldsymbol{V}}^{n+1}) + \boldsymbol{P}^{n+1}\boldsymbol{B}_p^T = \mathcal{F}_2^{n+1}, & (3.6b)\\ (-\boldsymbol{A}_p^T)\boldsymbol{U}^{n+1} + \boldsymbol{V}^{n+1}(-\boldsymbol{B}_p) = \boldsymbol{O}, & (3.6c)\\ \dfrac{1}{4\tau}\left(3\|\boldsymbol{U}^{n+1}\|_{l^2}^2 + 3\|\boldsymbol{V}^{n+1}\|_{l^2}^2 - 4\|\boldsymbol{U}^n\|_{l^2}^2 - 4\|\boldsymbol{V}^n\|_{l^2}^2 + \|\boldsymbol{U}^{n-1}\|_{l^2}^2 + \|\boldsymbol{V}^{n-1}\|_{l^2}^2\right) \\ + \theta\dfrac{3(q^{n+1})^2 - 4(q^n)^2 + (q^{n-1})^2}{2\tau} = \left(\dfrac{3\boldsymbol{U}^{n+1}-4\boldsymbol{U}^n+\boldsymbol{U}^{n-1}}{2\tau} + q^{n+1}\boldsymbol{F}_1(\tilde{\boldsymbol{U}}^{n+1},\tilde{\boldsymbol{V}}^{n+1}),\boldsymbol{U}^{n+1}\right)_{l^2} \\ + \left(\dfrac{3\boldsymbol{V}^{n+1}-4\boldsymbol{V}^n+\boldsymbol{V}^{n-1}}{2\tau} + q^{n+1}\boldsymbol{F}_2(\tilde{\boldsymbol{U}}^{n+1},\tilde{\boldsymbol{V}}^{n+1}),\boldsymbol{V}^{n+1}\right)_{l^2}. & (3.6d) \end{cases}$$

The implementation of the fully discrete DRLM schemes (3.5) and (3.6) can be carried out in the same manner as in the semi-discrete case and is thus omitted.

3.2. Fully discrete energy stability

In this subsection, we show that the fully discrete DRLM schemes (3.5) and (3.6) are also unconditionally energy stable.

Theorem 3.1. *In the absence of the external force $\boldsymbol{f}$, the fully discrete first-order DRLM scheme* (3.5) *is unconditionally stable in the sense that, for $n = 0, 1, \cdots, N_t - 1$,*

$$\frac{1}{2}\left(\|\boldsymbol{U}^{n+1}\|_{l^2}^2 + \|\boldsymbol{V}^{n+1}\|_{l^2}^2\right) + \theta\left[(q^{n+1})^2 - 1\right] \leq \frac{1}{2}\left(\|\boldsymbol{U}^n\|_{l^2}^2 + \|\boldsymbol{V}^n\|_{l^2}^2\right) + \theta\left[(q^n)^2 - 1\right].$$

Proof. Since $\boldsymbol{f} = [0,0]^T$, both $\mathcal{F}_1^{n+1}$ and $\mathcal{F}_2^{n+1}$ $(n \geq 0)$ are zero matrices. Taking the discrete l^2

inner product of (3.5a) and (3.5b) with $\boldsymbol{U}^{n+1}$ and $\boldsymbol{V}^{n+1}$, respectively, we obtain

$$\begin{aligned}
&\left(\frac{\boldsymbol{U}^{n+1}-\boldsymbol{U}^{n}}{\tau}+q^{n+1}\boldsymbol{F}_1(\boldsymbol{U}^{n},\boldsymbol{V}^{n}),\boldsymbol{U}^{n+1}\right)_{l^2}\\
&\qquad=\nu\left(\boldsymbol{A}_u\boldsymbol{U}^{n+1}+\boldsymbol{U}^{n+1}\boldsymbol{B}_u^T,\boldsymbol{U}^{n+1}\right)_{l^2}-(\boldsymbol{A}_p\boldsymbol{P}^{n+1},\boldsymbol{U}^{n+1})_{l^2}, \qquad (3.7)\\
&\left(\frac{\boldsymbol{V}^{n+1}-\boldsymbol{V}^{n}}{\tau}+q^{n+1}\boldsymbol{F}_2(\boldsymbol{U}^{n},\boldsymbol{V}^{n}),\boldsymbol{V}^{n+1}\right)_{l^2}\\
&\qquad=\nu\left(\boldsymbol{A}_v\boldsymbol{V}^{n+1}+\boldsymbol{V}^{n+1}\boldsymbol{B}_v^T,\boldsymbol{V}^{n+1}\right)_{l^2}-(\boldsymbol{P}^{n+1}\boldsymbol{B}_p^T,\boldsymbol{V}^{n+1})_{l^2}. \qquad (3.8)
\end{aligned}$$

For any matrices $\boldsymbol{A},\boldsymbol{B},\boldsymbol{X}$, and $\boldsymbol{Y}$, we have

$$(\boldsymbol{AX},\boldsymbol{Y})_{l^2}=h_xh_y\mathrm{Tr}\left((\boldsymbol{AX})^T\boldsymbol{Y}\right)=h_xh_y\mathrm{Tr}\left(\boldsymbol{X}^T\boldsymbol{A}^T\boldsymbol{Y}\right)=(\boldsymbol{X},\boldsymbol{A}^T\boldsymbol{Y})_{l^2}, \qquad (3.9)$$

$$(\boldsymbol{XB}^T,\boldsymbol{Y})_{l^2}=h_xh_y\mathrm{Tr}\left((\boldsymbol{XB}^T)^T\boldsymbol{Y}\right)=h_xh_y\mathrm{Tr}\left(\boldsymbol{BX}^T\boldsymbol{Y}\right)=h_xh_y\mathrm{Tr}\left(\boldsymbol{X}^T\boldsymbol{YB}\right)=(\boldsymbol{X},\boldsymbol{YB})_{l^2}, \qquad (3.10)$$

provided that the above matrix products are well-defined. Using (3.9)-(3.10) and the fact that $\boldsymbol{A}_p^T\boldsymbol{U}^{n+1}+\boldsymbol{V}^{n+1}\boldsymbol{B}_p=\boldsymbol{O}$ obtained from (3.5c), yields

$$\begin{aligned}
(\boldsymbol{A}_p\boldsymbol{P}^{n+1},\boldsymbol{U}^{n+1})_{l^2}+(\boldsymbol{P}^{n+1}\boldsymbol{B}_p^T,\boldsymbol{V}^{n+1})_{l^2}&=(\boldsymbol{P}^{n+1},\boldsymbol{A}_p^T\boldsymbol{U}^{n+1})_{l^2}+(\boldsymbol{P}^{n+1},\boldsymbol{V}^{n+1}\boldsymbol{B}_p)_{l^2}\\
&=(\boldsymbol{P}^{n+1},\boldsymbol{A}_p^T\boldsymbol{U}^{n+1}+\boldsymbol{V}^{n+1}\boldsymbol{B}_p)_{l^2}=0. \qquad (3.11)
\end{aligned}$$

It follows from the definitions of $\boldsymbol{A}_u$, $\boldsymbol{B}_v$, $\boldsymbol{A}_p$, and $\boldsymbol{B}_p$ (cf. (3.1)-(3.4)) that $\boldsymbol{A}_u=-\boldsymbol{A}_p\boldsymbol{A}_p^T$ and $\boldsymbol{B}_v=-\boldsymbol{B}_p\boldsymbol{B}_p^T$. Consequently,

$$\begin{aligned}
\left(\boldsymbol{A}_u\boldsymbol{U}^{n+1},\boldsymbol{U}^{n+1}\right)_{l^2}&=-\left(\boldsymbol{A}_p\boldsymbol{A}_p^T\boldsymbol{U}^{n+1},\boldsymbol{U}^{n+1}\right)_{l^2}\\
&=-\left(\boldsymbol{A}_p^T\boldsymbol{U}^{n+1},\boldsymbol{A}_p^T\boldsymbol{U}^{n+1}\right)_{l^2}=-\left\|\boldsymbol{A}_p^T\boldsymbol{U}^{n+1}\right\|_{l^2}^2\le 0, \qquad (3.12)\\
\left(\boldsymbol{V}^{n+1}\boldsymbol{B}_v^T,\boldsymbol{V}^{n+1}\right)_{l^2}&=-\left(\boldsymbol{V}^{n+1}\boldsymbol{B}_p\boldsymbol{B}_p^T,\boldsymbol{V}^{n+1}\right)_{l^2}\\
&=-\left(\boldsymbol{V}^{n+1}\boldsymbol{B}_p,\boldsymbol{V}^{n+1}\boldsymbol{B}_p\right)_{l^2}=-\left\|\boldsymbol{V}^{n+1}\boldsymbol{B}_p\right\|_{l^2}^2\le 0, \qquad (3.13)
\end{aligned}$$

where we have applied identities (3.9) and (3.10) to derive the above equalities. On the other hand, both $-\boldsymbol{B}_u$ and $-\boldsymbol{A}_v$ are symmetric positive definite matrices, they admit Cholesky decompositions $-\boldsymbol{B}_u=\boldsymbol{R}_u\boldsymbol{R}_u^T$ and $-\boldsymbol{A}_v=\boldsymbol{R}_v\boldsymbol{R}_v^T$. By using the same arguments as in (3.12) and (3.13), we obtain

$$\left(\boldsymbol{U}^{n+1}\boldsymbol{B}_u^T,\boldsymbol{U}^{n+1}\right)_{l^2}=-\left\|\boldsymbol{U}^{n+1}\boldsymbol{R}_u\right\|_{l^2}^2\le 0, \qquad (3.14)$$

$$\left(\boldsymbol{A}_v\boldsymbol{V}^{n+1},\boldsymbol{V}^{n+1}\right)_{l^2}=-\left\|\boldsymbol{R}_v^T\boldsymbol{V}^{n+1}\right\|_{l^2}^2\le 0. \qquad (3.15)$$

Combining (3.7)-(3.8) and (3.11)-(3.15) gives us

$$\left(\frac{\boldsymbol{U}^{n+1}-\boldsymbol{U}^{n}}{\tau}+q^{n+1}\boldsymbol{F}_1(\boldsymbol{U}^{n},\boldsymbol{V}^{n}),\boldsymbol{U}^{n+1}\right)_{l^2}+\left(\frac{\boldsymbol{V}^{n+1}-\boldsymbol{V}^{n}}{\tau}+q^{n+1}\boldsymbol{F}_2(\boldsymbol{U}^{n},\boldsymbol{V}^{n}),\boldsymbol{V}^{n+1}\right)_{l^2}\le 0.$$

This, together with (3.5d), leads to

$$\frac{1}{2\tau}\left(\|\boldsymbol{U}^{n+1}\|_{l^2}^2+\|\boldsymbol{V}^{n+1}\|_{l^2}^2-\|\boldsymbol{U}^{n}\|_{l^2}^2-\|\boldsymbol{V}^{n}\|_{l^2}^2\right)+\theta\frac{(q^{n+1})^2-(q^n)^2}{\tau}\le 0,$$

or equivalently,

$$\frac{1}{2}\left(\|\boldsymbol{U}^{n+1}\|_{l^2}^2+\|\boldsymbol{V}^{n+1}\|_{l^2}^2\right)+\theta(q^{n+1})^2\le\frac{1}{2}\left(\|\boldsymbol{U}^{n}\|_{l^2}^2+\|\boldsymbol{V}^{n}\|_{l^2}^2\right)+\theta(q^{n})^2,$$

which completes the proof of Theorem 3.1. □

Theorem 3.2. *In the absence of the external force $\boldsymbol{f}$, the fully discrete second-order DRLM scheme* (3.6) *is unconditionally stable in the sense that, for $n=1,2,\cdots,N_t-1$,*

$$\begin{aligned}&\frac{3}{4}\left(\|\boldsymbol{U}^{n+1}\|_{l^2}^2+\|\boldsymbol{V}^{n+1}\|_{l^2}^2\right)-\frac{1}{4}\left(\|\boldsymbol{U}^{n}\|_{l^2}^2+\|\boldsymbol{V}^{n}\|_{l^2}^2\right)+\theta\left[\frac{3}{2}(q^{n+1})^2-\frac{1}{2}(q^n)^2-1\right]\\&\quad\le\frac{3}{4}\left(\|\boldsymbol{U}^{n}\|_{l^2}^2+\|\boldsymbol{V}^{n}\|_{l^2}^2\right)-\frac{1}{4}\left(\|\boldsymbol{U}^{n-1}\|_{l^2}^2+\|\boldsymbol{V}^{n-1}\|_{l^2}^2\right)+\theta\left[\frac{3}{2}(q^{n})^2-\frac{1}{2}(q^{n-1})^2-1\right].\end{aligned}$$

Proof. By taking the discrete l^2 inner product of (3.6a) and (3.6b) with $\boldsymbol{U}^{n+1}$ and $\boldsymbol{V}^{n+1}$, respectively, and noting that $\mathcal{F}_1^{n+1}$ and $\mathcal{F}_2^{n+1}$ $(n\ge0)$ are zero matrices, we arrive at

$$\begin{aligned}&\left(\frac{3\boldsymbol{U}^{n+1}-4\boldsymbol{U}^{n}+\boldsymbol{U}^{n-1}}{2\tau}+q^{n+1}\boldsymbol{F}_1(\tilde{\boldsymbol{U}}^{n+1},\tilde{\boldsymbol{V}}^{n+1}),\boldsymbol{U}^{n+1}\right)_{l^2}\\&\qquad=\nu\left(\boldsymbol{A}_u\boldsymbol{U}^{n+1}+\boldsymbol{U}^{n+1}\boldsymbol{B}_u^T,\boldsymbol{U}^{n+1}\right)_{l^2}-(\boldsymbol{A}_p\boldsymbol{P}^{n+1},\boldsymbol{U}^{n+1})_{l^2},\\&\left(\frac{3\boldsymbol{V}^{n+1}-4\boldsymbol{V}^{n}+\boldsymbol{V}^{n-1}}{2\tau}+q^{n+1}\boldsymbol{F}_2(\tilde{\boldsymbol{U}}^{n+1},\tilde{\boldsymbol{V}}^{n+1}),\boldsymbol{V}^{n+1}\right)_{l^2}\\&\qquad=\nu\left(\boldsymbol{A}_v\boldsymbol{V}^{n+1}+\boldsymbol{V}^{n+1}\boldsymbol{B}_v^T,\boldsymbol{V}^{n+1}\right)_{l^2}-(\boldsymbol{P}^{n+1}\boldsymbol{B}_p^T,\boldsymbol{V}^{n+1})_{l^2}.\end{aligned}$$

Based on the proof of Theorem 3.1, we find that

$$\begin{aligned}&\nu\left(\boldsymbol{A}_u\boldsymbol{U}^{n+1}+\boldsymbol{U}^{n+1}\boldsymbol{B}_u^T,\boldsymbol{U}^{n+1}\right)_{l^2}-(\boldsymbol{A}_p\boldsymbol{P}^{n+1},\boldsymbol{U}^{n+1})_{l^2}\\&\quad+\nu\left(\boldsymbol{A}_v\boldsymbol{V}^{n+1}+\boldsymbol{V}^{n+1}\boldsymbol{B}_v^T,\boldsymbol{V}^{n+1}\right)_{l^2}-(\boldsymbol{P}^{n+1}\boldsymbol{B}_p^T,\boldsymbol{V}^{n+1})_{l^2}\le0.\end{aligned}$$

Therefore,

$$\begin{aligned}&\left(\frac{3\boldsymbol{U}^{n+1}-4\boldsymbol{U}^{n}+\boldsymbol{U}^{n-1}}{2\tau}+q^{n+1}\boldsymbol{F}_1(\tilde{\boldsymbol{U}}^{n+1},\tilde{\boldsymbol{V}}^{n+1}),\boldsymbol{U}^{n+1}\right)_{l^2}\\&\quad+\left(\frac{3\boldsymbol{V}^{n+1}-4\boldsymbol{V}^{n}+\boldsymbol{V}^{n-1}}{2\tau}+q^{n+1}\boldsymbol{F}_2(\tilde{\boldsymbol{U}}^{n+1},\tilde{\boldsymbol{V}}^{n+1}),\boldsymbol{V}^{n+1}\right)_{l^2}\le0.\end{aligned}\tag{3.16}$$

The combination of (3.6d) and (3.16) results in

$$\begin{aligned}&\frac{1}{4\tau}\left(3\|\boldsymbol{U}^{n+1}\|_{l^2}^2+3\|\boldsymbol{V}^{n+1}\|_{l^2}^2-4\|\boldsymbol{U}^{n}\|_{l^2}^2-4\|\boldsymbol{V}^{n}\|_{l^2}^2+\|\boldsymbol{U}^{n-1}\|_{l^2}^2+\|\boldsymbol{V}^{n-1}\|_{l^2}^2\right)\\&\qquad+\theta\frac{3(q^{n+1})^2-4(q^n)^2+(q^{n-1})^2}{2\tau}\le0.\end{aligned}$$

This implies that

$$\begin{aligned}&\frac{3}{4}\left(\|\boldsymbol{U}^{n+1}\|_{l^2}^2+\|\boldsymbol{V}^{n+1}\|_{l^2}^2\right)-\frac{1}{4}\left(\|\boldsymbol{U}^{n}\|_{l^2}^2+\|\boldsymbol{V}^{n}\|_{l^2}^2\right)+\theta\left[\frac{3}{2}(q^{n+1})^2-\frac{1}{2}(q^n)^2\right]\\&\quad\le\frac{3}{4}\left(\|\boldsymbol{U}^{n}\|_{l^2}^2+\|\boldsymbol{V}^{n}\|_{l^2}^2\right)-\frac{1}{4}\left(\|\boldsymbol{U}^{n-1}\|_{l^2}^2+\|\boldsymbol{V}^{n-1}\|_{l^2}^2\right)+\theta\left[\frac{3}{2}(q^{n})^2-\frac{1}{2}(q^{n-1})^2\right],\end{aligned}$$

which concludes the proof of Theorem 3.2. □

Remark 3.1. *(i) Let $\mathcal{E}_1^n$ and $\mathcal{E}_2^n$ ($n \geq 1$) be the discrete error functions for q associated with the first- and second-order DRLM schemes:*

$$\mathcal{E}_1^n(q^n, \theta) := \theta \left[(q^n)^2 - 1 \right], \quad \mathcal{E}_2^n(q^n, q^{n-1}, \theta) := \theta \left[\frac{3}{2}(q^n)^2 - \frac{1}{2}(q^{n-1})^2 - 1 \right].$$

Under suitable choices of θ, it will be demonstrated in the numerical experiments (cf. Section 4) that both $\mathcal{E}_1^n$ and $\mathcal{E}_2^n$ are significantly smaller than the main energy functional. Therefore, they can be considered negligible in Theorems 2.1 and 2.2 (for the semi-discrete case) and Theorems 3.1 and 3.2 (for the fully discrete case).

(ii) The energy stability of the proposed DRLM schemes remains valid under certain mixed boundary conditions. One typical example is the 2D Kelvin-Helmholtz instability (cf. Subsection 4.4), where periodic conditions are applied along the vertical boundaries while free-slip conditions are imposed at the horizontal boundaries.

(iii) Due to the coupling between the Lagrange multiplier, velocity, and pressure, the fully discrete convergence analysis of the proposed DRLM schemes (3.5) *and* (3.6) *is challenging and remains an open problem. We refer to [22] and [5] for error analysis of the MAC method applied to the NS equations and other coupled physical systems involving fluid motion, such as the Cahn-Hilliard-Hele-Shaw equation.*

3.3. Preconditioned iterative solvers for generalized Stokes systems

The proposed first- and second-order DRLM schemes involve solving the following generalized Stokes system at each time step (cf. (2.8), (2.9), (2.12), and (2.13)):

$$\begin{cases} \alpha \boldsymbol{u} - \nu \Delta \boldsymbol{u} + \nabla p = \boldsymbol{g}, & \text{(3.17a)} \\ \nabla \cdot \boldsymbol{u} = 0, & \text{(3.17b)} \end{cases}$$

where $\boldsymbol{u} = [u, v]^T$ and p denote the velocity field and pressure, ν is the viscosity coefficient, $\boldsymbol{g} = [g_1, g_2]^T$ is a given vector function, $\alpha = \frac{1}{\tau}$ for the first-order DRLM scheme, and $\alpha = \frac{3}{2\tau}$ for the second-order DRLM scheme. After spatial discretization on the MAC staggered grid, system (3.17) becomes

$$\begin{cases} \alpha \boldsymbol{U} - \nu(\boldsymbol{A}_u \boldsymbol{U} + \boldsymbol{U} \boldsymbol{B}_u^T) + \boldsymbol{A}_p \boldsymbol{P} = \mathcal{G}_1, & \text{(3.18a)} \\ \alpha \boldsymbol{V} - \nu(\boldsymbol{A}_v \boldsymbol{V} + \boldsymbol{V} \boldsymbol{B}_v^T) + \boldsymbol{P} \boldsymbol{B}_p^T = \mathcal{G}_2, & \text{(3.18b)} \\ (-\boldsymbol{A}_p^T)\boldsymbol{U} + \boldsymbol{V}(-\boldsymbol{B}_p) = \boldsymbol{O}, & \text{(3.18c)} \end{cases}$$

where $\boldsymbol{U}, \boldsymbol{V}$, and $\boldsymbol{P}$ are the approximations of u, v, and p over $\Omega_{h,u}, \Omega_{h,v}$, and $\Omega_{h,p}$, respectively; $\mathcal{G}_1$ and $\mathcal{G}_2$ are the values of g_1 and g_2 over $\Omega_{h,u}$ and $\Omega_{h,v}$, respectively. The matrices $\boldsymbol{A}_u, \boldsymbol{B}_u, \boldsymbol{A}_v, \boldsymbol{B}_v, \boldsymbol{A}_p$, and $\boldsymbol{B}_p$ are defined in (3.1)-(3.4).

System (3.18) can be transformed into the following saddle point problem:

$$\begin{bmatrix} \boldsymbol{A} & \boldsymbol{B}^T \\ \boldsymbol{B} & \boldsymbol{O} \end{bmatrix} \begin{bmatrix} \boldsymbol{x} \\ \boldsymbol{y} \end{bmatrix} = \begin{bmatrix} \mathcal{G} \\ \boldsymbol{O} \end{bmatrix}, \tag{3.19}$$

where $\boldsymbol{x} = \begin{bmatrix} \mathrm{vec}(\boldsymbol{U}) \\ \mathrm{vec}(\boldsymbol{V}) \end{bmatrix}$, $\boldsymbol{y} = \mathrm{vec}(\boldsymbol{P})$, and $\mathcal{G} = \begin{bmatrix} \mathrm{vec}(\mathcal{G}_1) \\ \mathrm{vec}(\mathcal{G}_2) \end{bmatrix}$, with vec denoting the vectorization operator. The coefficient matrix $\boldsymbol{A}$ is defined as

$$\boldsymbol{A} = \begin{bmatrix} \alpha \boldsymbol{I}_{(N_x-1)N_y} - \nu(\boldsymbol{I}_{N_y} \otimes \boldsymbol{A}_u + \boldsymbol{B}_u \otimes \boldsymbol{I}_{N_x-1}) & \boldsymbol{O} \\ \boldsymbol{O} & \alpha \boldsymbol{I}_{N_x(N_y-1)} - \nu(\boldsymbol{I}_{N_y-1} \otimes \boldsymbol{A}_v + \boldsymbol{B}_v \otimes \boldsymbol{I}_{N_x}) \end{bmatrix},$$

for the homogeneous Dirichlet boundary condition, and

$$\boldsymbol{A} = \begin{bmatrix} \alpha \boldsymbol{I}_{N_x N_y} - \nu(\boldsymbol{I}_{N_y} \otimes \boldsymbol{A}_u + \boldsymbol{B}_u \otimes \boldsymbol{I}_{N_x}) & \boldsymbol{O} \\ \boldsymbol{O} & \alpha \boldsymbol{I}_{N_x N_y} - \nu(\boldsymbol{I}_{N_y} \otimes \boldsymbol{A}_v + \boldsymbol{B}_v \otimes \boldsymbol{I}_{N_x}) \end{bmatrix},$$

for the periodic boundary condition, where $\otimes$ denotes the Kronecker product. The matrix $\boldsymbol{B}$ is given by:

$$\boldsymbol{B} = \begin{bmatrix} \boldsymbol{I}_{N_y} \otimes \boldsymbol{A}_p^T & \boldsymbol{B}_p^T \otimes \boldsymbol{I}_{N_x} \end{bmatrix}.$$

Since the pressure p is defined up to a constant, $\boldsymbol{B}^T$ has a one-dimensional kernel. By fixing $\boldsymbol{P}(1,1) = 0$, we may assume without loss of generality that $\boldsymbol{B}^T$ has full rank.

Suppose that $\boldsymbol{A} \in \mathbb{R}^{n \times n}$, $\boldsymbol{B} \in \mathbb{R}^{m \times n}$ (with $m < n$), and that $\boldsymbol{A}$ is decomposed as $\boldsymbol{A} = \boldsymbol{D} - \boldsymbol{E}$, where $\boldsymbol{D}$ is the diagonal matrix obtained from $\boldsymbol{A}$. Let $\hat{\boldsymbol{S}} = \boldsymbol{B}\boldsymbol{D}^{-1}\boldsymbol{B}^T$ be an approximation of the Schur complement matrix $\boldsymbol{S} = \boldsymbol{B}\boldsymbol{A}^{-1}\boldsymbol{B}^T$. As discussed in [3, 9], we consider the following block preconditioner:

$$\begin{bmatrix} \boldsymbol{D} & \boldsymbol{B}^T \\ \boldsymbol{B} & \boldsymbol{O} \end{bmatrix}^{-1} = \begin{bmatrix} (\boldsymbol{I}_n - \boldsymbol{D}^{-1}\boldsymbol{B}^T\hat{\boldsymbol{S}}^{-1}\boldsymbol{B})\boldsymbol{D}^{-1} & \boldsymbol{D}^{-1}\boldsymbol{B}^T\hat{\boldsymbol{S}}^{-1} \\ \hat{\boldsymbol{S}}^{-1}\boldsymbol{B}\boldsymbol{D}^{-1} & -\hat{\boldsymbol{S}}^{-1} \end{bmatrix}. \tag{3.20}$$

Preconditioning (3.19) from the left by (3.20) yields

$$\begin{bmatrix} \boldsymbol{I}_n - (\boldsymbol{I}_n - \boldsymbol{D}^{-1}\boldsymbol{B}^T\hat{\boldsymbol{S}}^{-1}\boldsymbol{B})\boldsymbol{D}^{-1}\boldsymbol{E} & \boldsymbol{O} \\ -\hat{\boldsymbol{S}}^{-1}\boldsymbol{B}\boldsymbol{D}^{-1}\boldsymbol{E} & \boldsymbol{I}_m \end{bmatrix} \begin{bmatrix} \boldsymbol{x} \\ \boldsymbol{y} \end{bmatrix} = \begin{bmatrix} (\boldsymbol{I}_n - \boldsymbol{D}^{-1}\boldsymbol{B}^T\hat{\boldsymbol{S}}^{-1}\boldsymbol{B})\boldsymbol{D}^{-1}\mathcal{G} \\ \hat{\boldsymbol{S}}^{-1}\boldsymbol{B}\boldsymbol{D}^{-1}\mathcal{G} \end{bmatrix}. \tag{3.21}$$

Therefore, solving (3.19) or (3.21) is equivalent to performing the following two steps:

(i) Solve for $\boldsymbol{x}$ the linear system

$$\left[\boldsymbol{I}_n - (\boldsymbol{I}_n - \boldsymbol{D}^{-1}\boldsymbol{B}^T\hat{\boldsymbol{S}}^{-1}\boldsymbol{B})\boldsymbol{D}^{-1}\boldsymbol{E}\right]\boldsymbol{x} = (\boldsymbol{I}_n - \boldsymbol{D}^{-1}\boldsymbol{B}^T\hat{\boldsymbol{S}}^{-1}\boldsymbol{B})\boldsymbol{D}^{-1}\mathcal{G}. \tag{3.22}$$

(ii) Compute $\boldsymbol{y}$ from $\boldsymbol{x}$ by $\boldsymbol{y} = \hat{\boldsymbol{S}}^{-1}\boldsymbol{B}\boldsymbol{D}^{-1}(\boldsymbol{E}\boldsymbol{x} + \mathcal{G})$.

The linear system (3.22) can be solved using various iterative solvers; in the numerical experiments, we employ the GMRES method. It is worth noting that $\hat{\boldsymbol{S}} \in \mathbb{R}^{m \times m}$ is a sparse symmetric positive definite matrix, allowing efficient computation of $\hat{\boldsymbol{S}}^{-1}\boldsymbol{z}$ for any $\boldsymbol{z} \in \mathbb{R}^m$, such as via the incomplete Cholesky decomposition.

4. Numerical experiments

In this section, we carry out several numerical experiments to verify the accuracy and energy stability of the proposed first- and second-order DRLM schemes with difference choices of the regularization parameter and Reynolds number. Various benchmark test cases in 2D and 3D, including lid-driven cavity flow and Kelvin-Helmholtz instability, are also considered to validate the performance of the proposed schemes, particularly the second-order one. For simplicity, we choose the uniform MAC spatial mesh size $h = h_x = h_y$ in 2D and $h = h_x = h_y = h_z$ in 3D. Unless otherwise stated, the viscosity coefficient is defined as $\nu = \frac{1}{Re}$ for a given Reynolds number Re.

4.1. Convergence test

We set the spatial domain $\Omega = (0,1)^2$ and the final time $T = 1$. The external force $\boldsymbol{f}$ is computed according to the following analytic solution [19], whose velocity satisfies homogeneous Dirichlet boundary conditions:

$$\begin{cases} p(x,y,t) = \cos(\pi x)\sin(\pi y)\sin(t), \\ u(x,y,t) = \pi \sin^2(\pi x)\sin(2\pi y)\sin(t), \\ v(x,y,t) = -\pi \sin(2\pi x)\sin^2(\pi y)\sin(t). \end{cases}$$

We first consider the case $Re = 10$ (i.e., $\nu = 0.1$). To study the convergence of the DRLM schemes, we vary both the spatial mesh size and time step size with $h = \dfrac{\tau}{8}$ and $\tau \in \left\{\frac{1}{8}, \frac{1}{16}, \frac{1}{32}, \frac{1}{64}\right\}$. The L^2 errors of the velocity and pressure, as well as the absolute errors of the Lagrange multiplier q with different values of $\theta \in \{10^{-2}, 10^{-1}, 1, 10, 10^2\}$ are shown in Figure 2 for both first- and second-order DRLM schemes. We observe that the errors in velocity, pressure, and q are large for small values of θ, such as $\theta \in \{10^{-2}, 10^{-1}\}$. We remark that when $\theta = 10^{-3}$ and $\tau \in \{\frac{1}{8}, \frac{1}{16}\}$, the second-order scheme produces complex values for q after a certain number of iterations; therefore, we do not consider $\theta = 10^{-3}$ in this case. Conversely, when $\theta \in \{1, 10, 10^2\}$, q stabilizes closer to 1, resulting in the expected convergence rates for the proposed schemes. This highlights the critical role of θ in our DRLM formulations: if θ is too small or absent, the schemes produce incorrect solutions, but they perform significantly better when θ is large enough, with a minimum value of 1.

Next, we increase the Reynolds number to $Re = 1000$ (i.e., $\nu = 0.001$). Due to the explicit treatment of the convection term which requires some CFL condition, we consider $h = 4\tau$ and $\tau \in \left\{\frac{1}{128}, \frac{1}{256}, \frac{1}{512}, \frac{1}{1024}\right\}$. The corresponding errors of the velocity, pressure, and Lagrange multiplier for different values of $\theta \in \{10^{-3}, 10^{-2}, 10^{-1}, 1, 10\}$ are presented in Figure 3. As θ increases, errors of the concerned quantities become smaller, and both first- and second-order DRLM schemes exhibit the correct order of convergence when $\theta \geq 1$. Note that the results with $\theta = 10^2$ are almost identical to those with $\theta = 10$, thus omitted here. Moreover, for this case with a large Reynolds number, $\theta = 10^{-3}$ could be used without leading to complex values for q; nevertheless, the expected accuracy of the numerical solution is only achieved when θ is sufficiently large.

4.2. Energy dissipation test

We now examine the Taylor-Green vortex problem in $\Omega = (0,1)^2$ with zero external force, $\boldsymbol{f} = [0,0]^T$, and the periodic boundary conditions. The exact solution to this problem is given by

$$\begin{cases} u(x,y,t) = \sin(2\pi x)\cos(2\pi y)e^{-8\pi^2\nu t}, \\ v(x,y,t) = -\cos(2\pi x)\sin(2\pi y)e^{-8\pi^2\nu t}, \\ p(x,y,t) = \dfrac{1}{4}\left[\cos(4\pi x) + \cos(4\pi y)\right] e^{-16\pi^2\nu t}. \end{cases}$$

The original kinetic energy can be computed explicitly as follows:

$$\mathcal{K}(\boldsymbol{u}(t)) = \frac{1}{2}\int_\Omega \left[u^2(x,y,t) + v^2(x,y,t)\right] dxdy = \frac{1}{4}e^{-16\pi^2\nu t}.$$

We set $T = 20$, $Re = 1000$, and $h = 1.5\tau = 0.01$. The evolutions of $\mathcal{K}(\boldsymbol{u}^n)$, $\mathcal{K}(\boldsymbol{u})$, and $\mathcal{E}_i^n$ $(i = 1, 2)$ generated by the first- and second-order DRLM schemes with $\theta \in \{1, 100\}$ are shown in Figure 4,

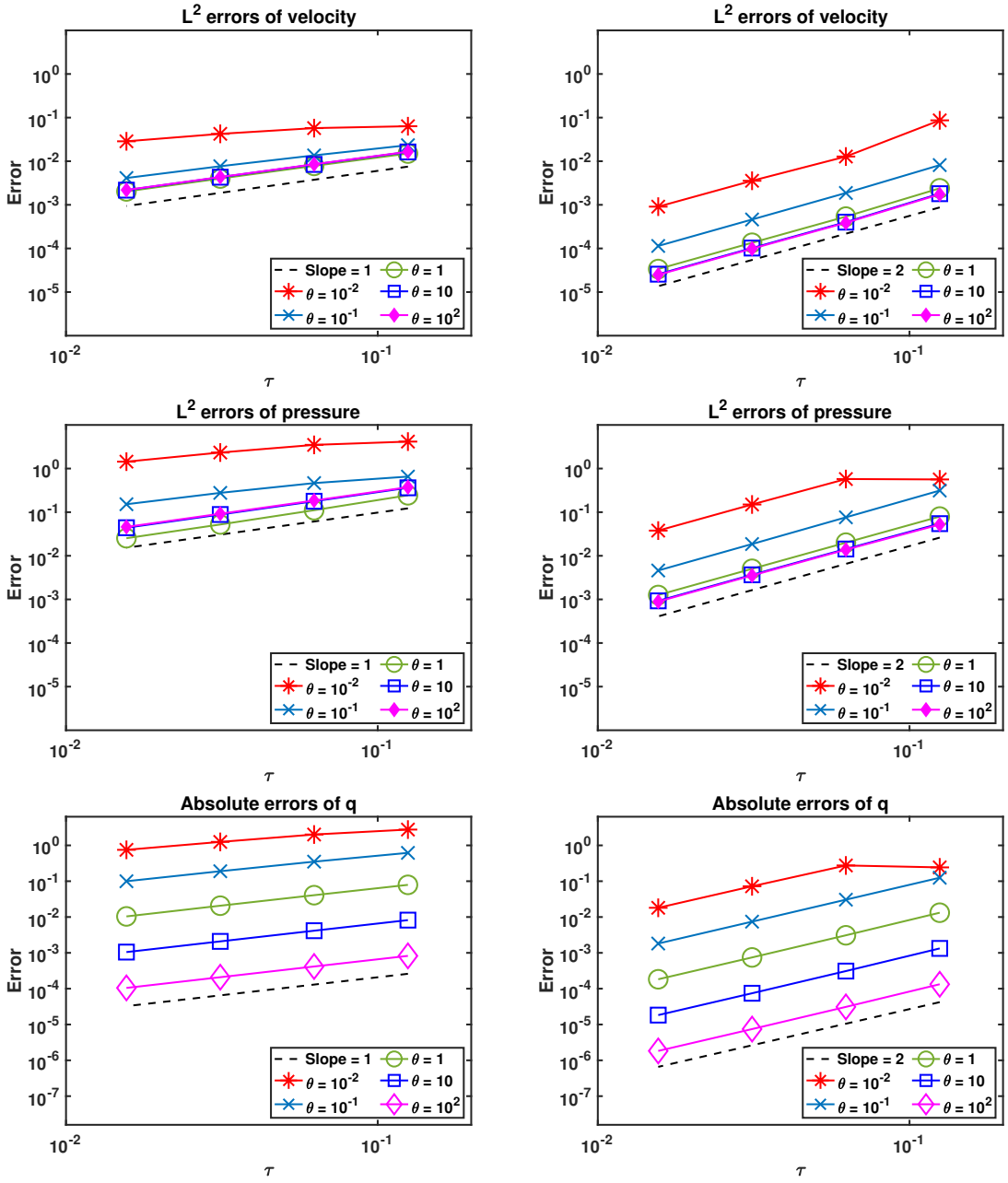

Figure 2: [Convergence test, $Re = 10$] Errors of the velocity, pressure, and Lagrange multiplier by the first-order (left) and second-order (right) DRLM schemes with $h = \frac{\tau}{8}$ and difference values of θ.

where we clearly observe the energy decay property of the numerical solutions. Figure 4 also confirms that the additional terms, $\mathcal{E}_1^n$ and $\mathcal{E}_2^n$, in our energy stability analysis (cf. Theorems 2.1-2.2 and 3.1-3.2) are negligible due to their small magnitudes. Furthermore, the results for $\theta = 1$ and $\theta = 100$ are quite similar, with the second-order DRLM scheme exhibiting better performance.

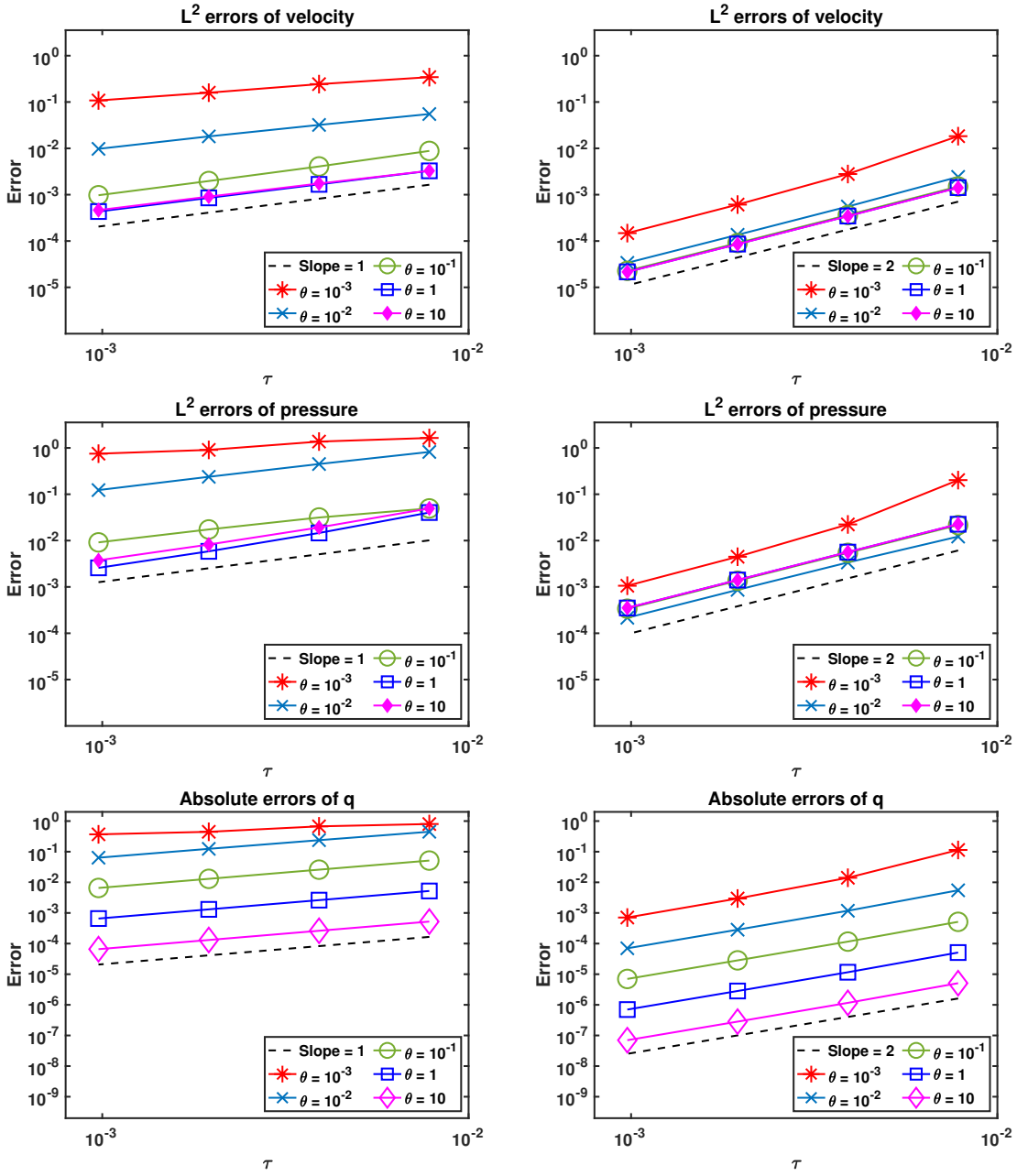

Figure 3: [Convergence test, $Re = 1000$] Errors of the velocity, pressure, and Lagrange multiplier by the first-order (left) and second-order (right) DRLM schemes with $h = 4\tau$ and difference values of θ.

4.3. Lid-driven cavity flow

Next, we demonstrate the accuracy of our new schemes through realistic physical simulations, the well-known lid-driven cavity flow [11, 19, 21, 23] in 2D and [2, 20, 41, 14] in 3D. For the 2D problem, the computational domain $\Omega = (0, 1)^2$ consists of three rigid walls (at $x = 0$, $x = 1$, and $y = 0$) with no-slip boundary conditions and a lid (at $y = 1$) moving with a tangential unit velocity. Since the exact solution to this problem is not available, we compare our numerical results with

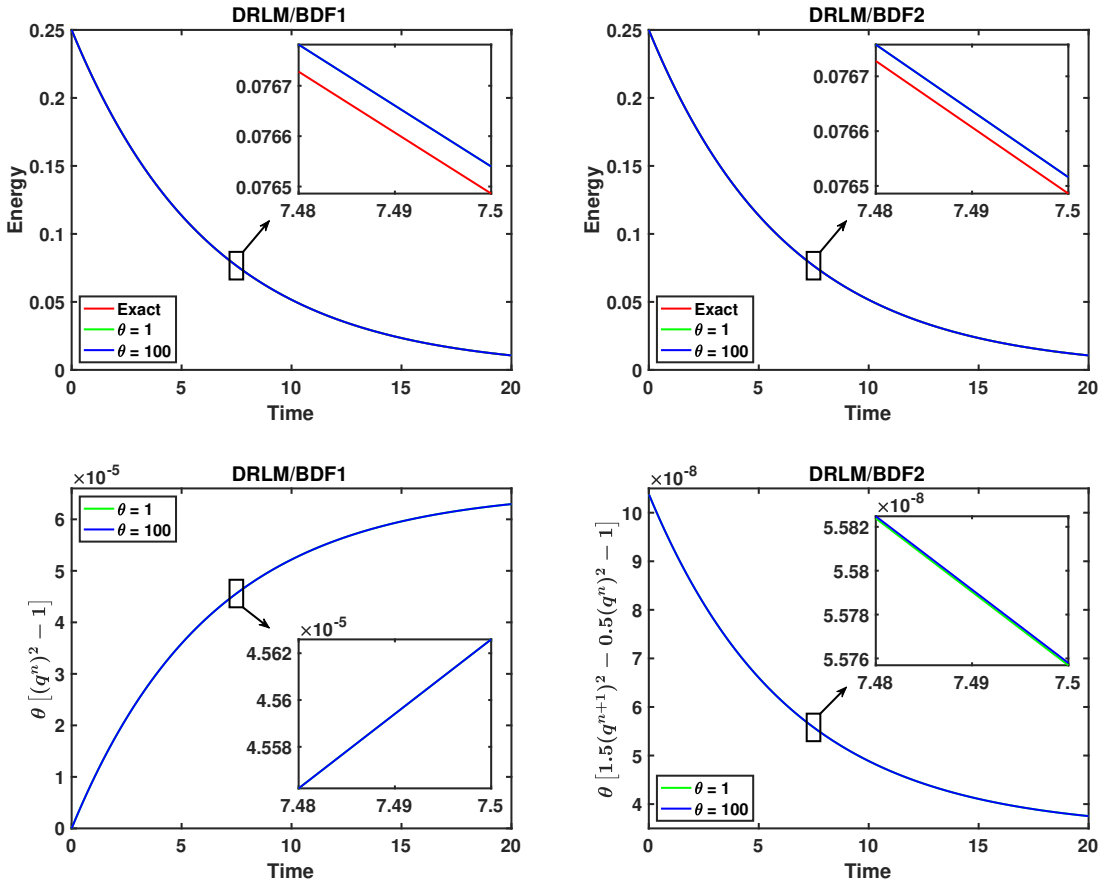

Figure 4: [Taylor-Green vortex, $Re = 1000$] Evolution of the energy functional and error function $\mathcal{E}_i^n$ $(i = 1, 2)$ by the first-order (left) and second-order (right) DRLM schemes with $h = 1.5\tau = 0.01$.

the benchmark method in [11]. Using the second-order DRLM scheme with $Re = 5000$, $\theta = 100$, and $h = 2\tau = \frac{1}{256}$, we perform the simulation until the steady state is reached, characterized by $\|\boldsymbol{u}^n - \boldsymbol{u}^{n-1}\|_\infty \leq 10^{-6}$. Contour plots of the velocity magnitude at times $t = 4$, $t = 6$, and $t = 10$ are presented in Figure 5. Figure 6 illustrates the velocity magnitude, vorticity, and stream function at the final steady state, along with velocity components at the cavity centerlines, which closely match the benchmark results [11]. As reported in [11] and [19], in addition to the primary and secondary vortices at the bottom corners, a third vortex emerges in the upper left corner at $Re = 5000$. Thus, our numerical simulation based on the DRLM approach accurately captures the dynamic evolution of the velocity field, achieving the steady state that compares well with existing results.

We proceed to consider the 3D lid-driven flow in a cubic cavity $\Omega = (0, 1)^3$, a natural extension of the 2D driven cavity test case. The fluid is initially at rest and starts moving as the top lid (at $y = 1$) is dragged at a constant unit speed in the positive x-direction. On all other sides, the velocity satisfies homogeneous Dirichlet boundary conditions. With $Re = 1000$, $\theta = 100$, and $h = 1.5\tau = 0.01$ fixed, we simulate the flow evolution using the second-order DRLM scheme until the steady state is achieved, indicated by $\|\boldsymbol{u}^n - \boldsymbol{u}^{n-1}\| \leq 10^{-6}$. Figure 7 displays contour plots of the vorticity components $[\omega_1, \omega_2, \omega_3]^T = \nabla \times \boldsymbol{u}$ on the midplanes $x = 0.5$, $y = 0.5$, and $z = 0.5$,

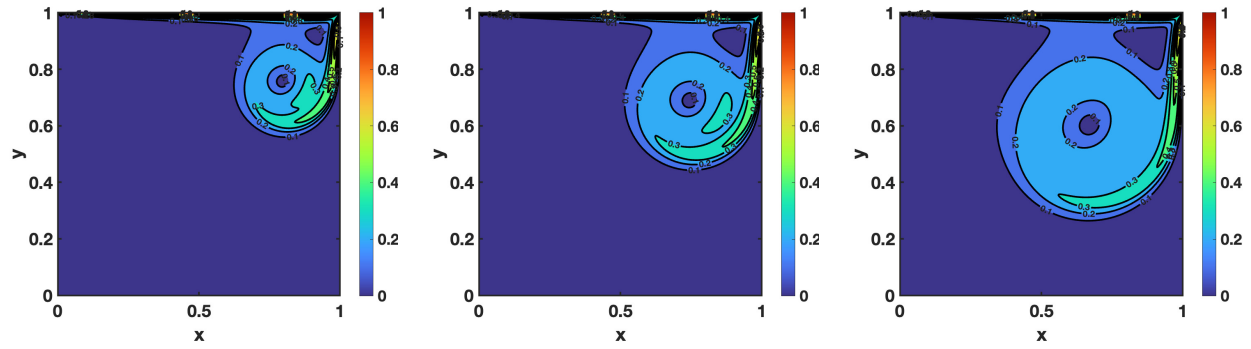

Figure 5: [2D lid-driven cavity, $Re = 5000$] Contour plots of the velocity magnitude at times $t = 4, 6$, and 10 by the second-order DRLM scheme with $h = 2\tau = \frac{1}{256}$.

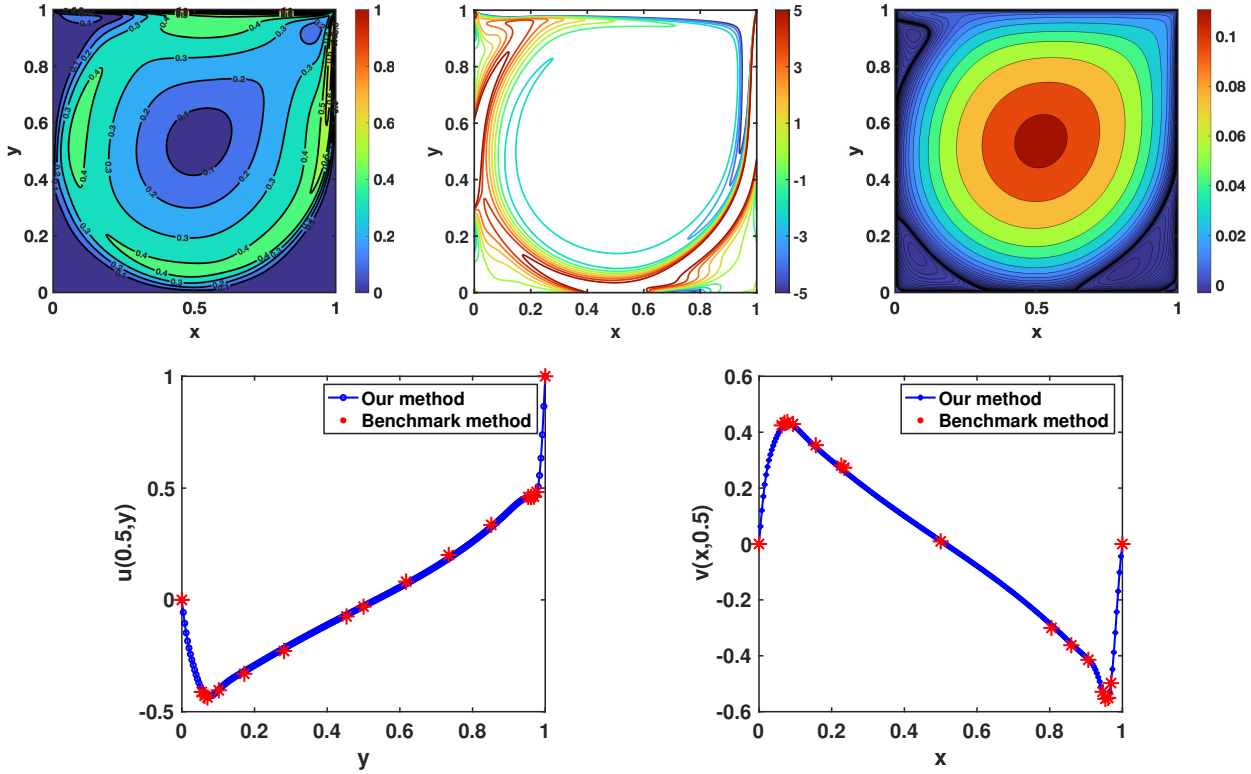

Figure 6: [2D lid-driven cavity, $Re = 5000$] Contour plots of the velocity magnitude, vorticity, and stream function (top) and the velocity components along the centerlines (bottom) at the steady state by the second-order DRLM scheme with $h = 2\tau = \frac{1}{256}$.

respectively. The flow is symmetric about the plane $z = 0.5$, and the presence of Taylor-Görtler-like vortices in the bottom region of the cavity is observed besides corner vortices, which are consistent with those reported in [17, 28]. The distributions of the u- and v-velocity components along the vertical ($x = z = 0.5$) and horizontal ($y = z = 0.5$) plane centerlines are provided in Figure 8, demonstrating strong agreement with the benchmark results [2].

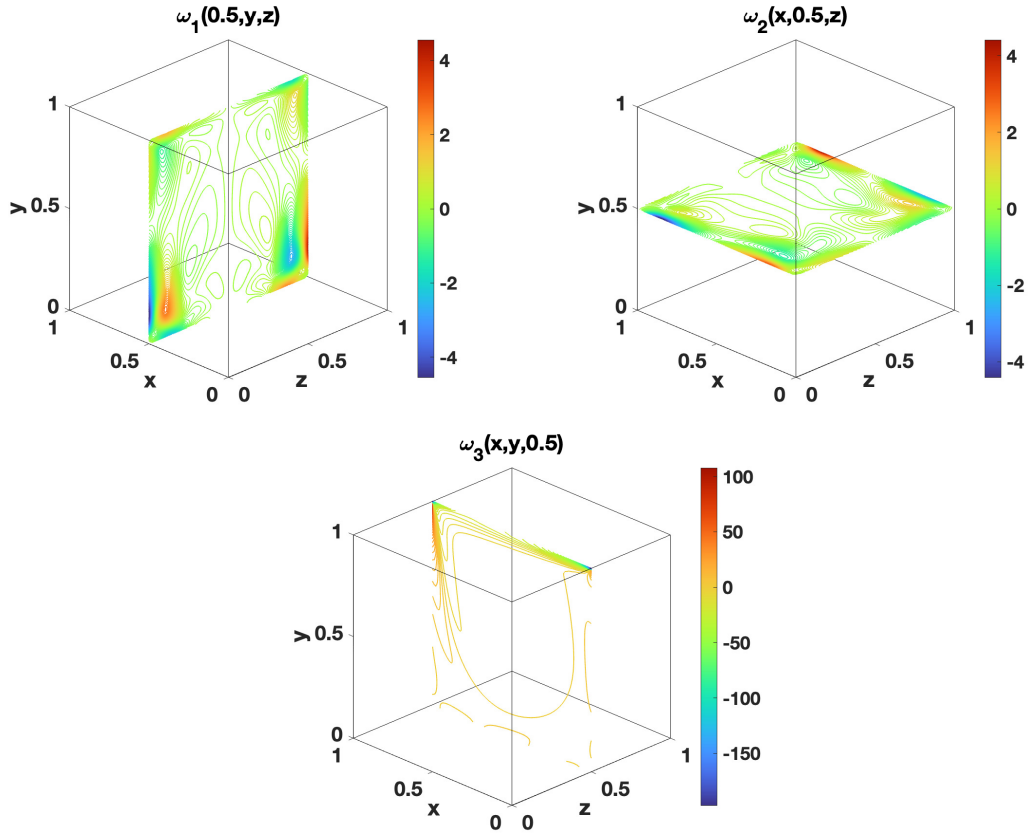

Figure 7: [3D lid-driven cavity, $Re = 1000$] Contour plots of the vorticity components on the midplanes at the steady state by the second-order DRLM scheme with $h = 1.5\tau = 0.01$.

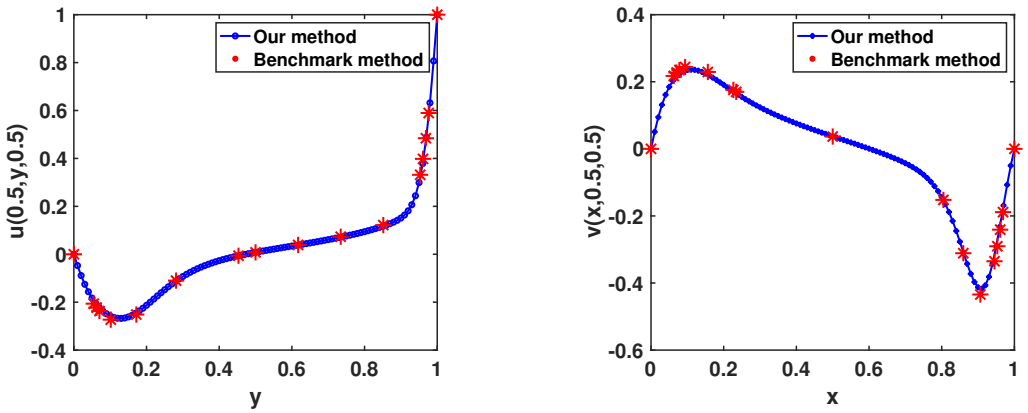

Figure 8: [3D lid-driven cavity, $Re = 1000$] Velocity components along the centerlines at the steady state by the second-order DRLM scheme with $h = 1.5\tau = 0.01$.

4.4. Kelvin–Helmholtz instability

When there is an initial velocity difference across a shear layer, small disturbances can grow over time, leading to the formation of vortices. This phenomenon is known as the Kelvin-Helmholtz

instability. We consider the 2D NS equations in $\Omega = (0,1)^2$ with $\boldsymbol{f} = [0,0]^T$. At the top and bottom boundaries of the domain Ω, we apply the conditions $\frac{\partial u}{\partial y} = 0$ and $v = 0$, while at the left and right sides of Ω, we impose periodic boundary conditions. Since no body forces are present, the entire motion is driven by the initial condition, which is given by [31]:

$$\boldsymbol{u}_0(x,y) = \begin{bmatrix} u_\infty \tanh\left(\frac{2y-1}{\delta_0}\right) \\ 0 \end{bmatrix} + c_n \begin{bmatrix} \partial_y \psi(x,y) \\ -\partial_x \psi(x,y) \end{bmatrix},$$

with the corresponding stream function

$$\psi(x,y) = u_\infty \exp\left(-\frac{(y-0.5)^2}{\delta_0^2}\right)\left[\cos(8\pi x) + \cos(20\pi x)\right].$$

Here, $\delta_0 = \frac{1}{28}$ denotes the initial vorticity thickness, $u_\infty = 1$ is a reference velocity, and $c_n = 10^{-3}$ is a scaling factor. With fixed Reynolds number $Re = 100$, the kinematic viscosity is given by $\nu = \frac{\delta_0 u_\infty}{Re} = \frac{1}{2800}$. We take $h = \frac{1}{256}$, $\tau = \frac{1}{560}$, $\theta = 100$, and $T = 200\bar{t}$ with $\bar{t} = \frac{\delta_0}{u_\infty} = \frac{1}{28}$ being the time unit. Evolution of the vorticity produced by the second-order DRLM scheme at different times is illustrated in Figure 9. We observe that four vortices gradually emerge from the initial condition, exhibiting instability and a tendency to merge into two larger vortices. These two ellipsoidal vortices remain separated for a long time, with their magnitudes decreasing until the final time $T = 200\bar{t}$. Figure 10 confirms the energy dissipation of the system, in agreement with the benchmark results [31], and shows the evolution of the discrete error function $\mathcal{E}_2^n$, which remains insignificant compared to the total energy.

5. Conclusions

In this work, we proposed a novel approach for solving the incompressible NS equations. By introducing a dynamic equation involving the original energy, a Lagrange multiplier, and a regularization parameter, the NS equations are reformulated into an equivalent system. Based on the BDF method with an explicit treatment of the nonlinear convection, the first- and second-order DRLM schemes were derived and shown to unconditionally satisfy the energy dissipation law. Fully discrete energy stability was also carried out with the MAC spatial discretization. Unlike existing Lagrange multiplier methods, the presence of the regularization parameter in the DRLM formulation enables the use of large time step sizes while still ensuring the uniqueness of the Lagrange multiplier and therefore the numerical solutions. Our numerical schemes are linear and easy to implement, as they only require solving two generalized Stokes systems and a quadratic equation at each time step. To further enhance the overall performance of the DRLM approach, we provided efficient preconditioned iterative solvers for generalized Stokes systems. Various numerical experiments in 2D and 3D were conducted to verify the convergence, energy stability, and the efficiency of the proposed DRLM schemes. Future research includes fully discrete error analysis of the DRLM schemes as well as application of the DRLM methods to other types of PDEs, such as the coupled Cahn-Hilliard-Navier-Stokes system. Extension of the current approach to higher order DRLM schemes using the BDF method will also be investigated; we refer to [10] for a discussion of high-order BDF schemes with time filters and to [16] for the development of energy stable SAV-BDF schemes up to fifth-order accuracy in time.

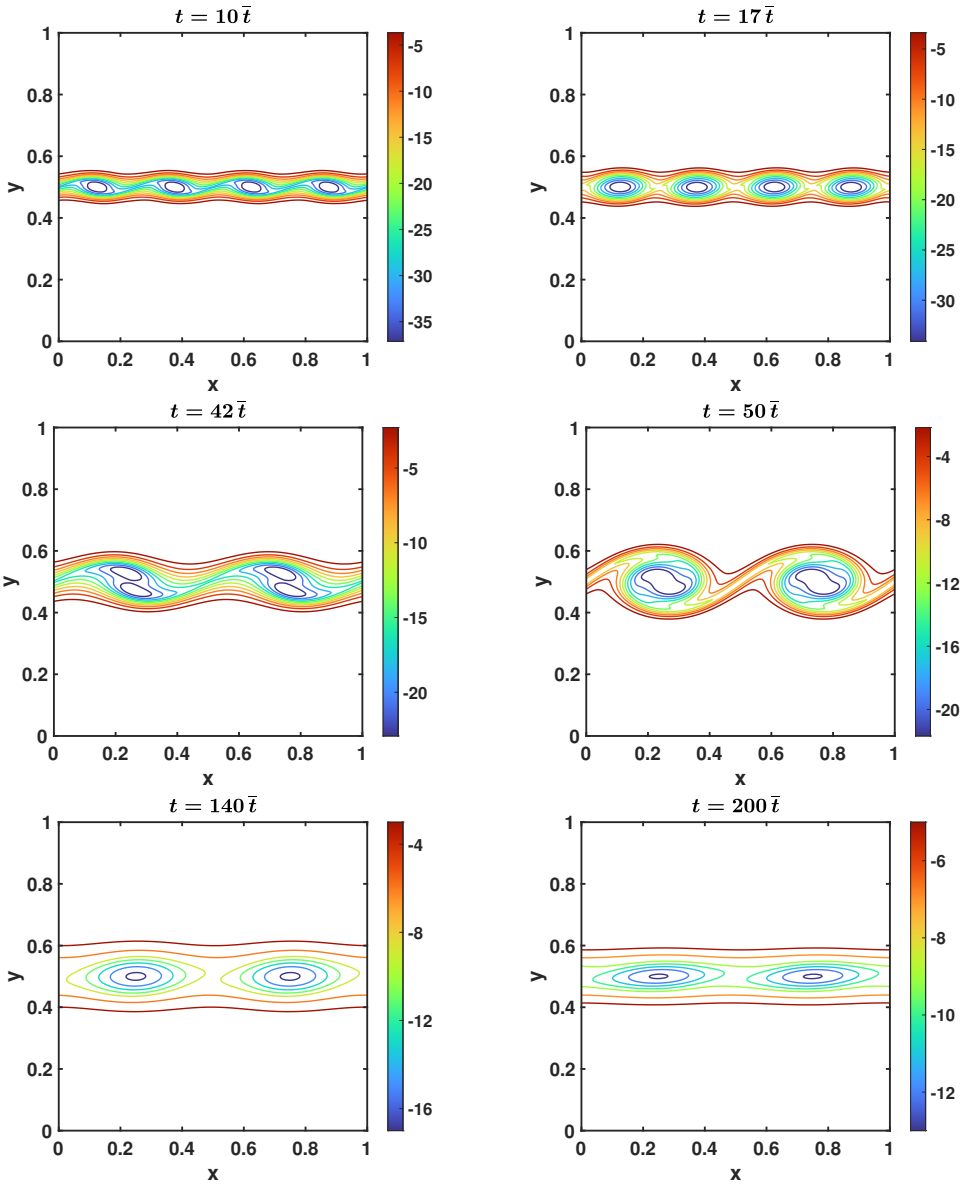

Figure 9: [Kelvin-Helmholtz instability, $Re = 100$] Evolution of the vorticity at different times $t = 10\bar{t}$, $17\bar{t}$, $42\bar{t}$, $50\bar{t}$, $140\bar{t}$, and $200\bar{t}$ by the second-order DRLM scheme with $h = \frac{1}{256}$ and $\tau = \frac{1}{560}$.

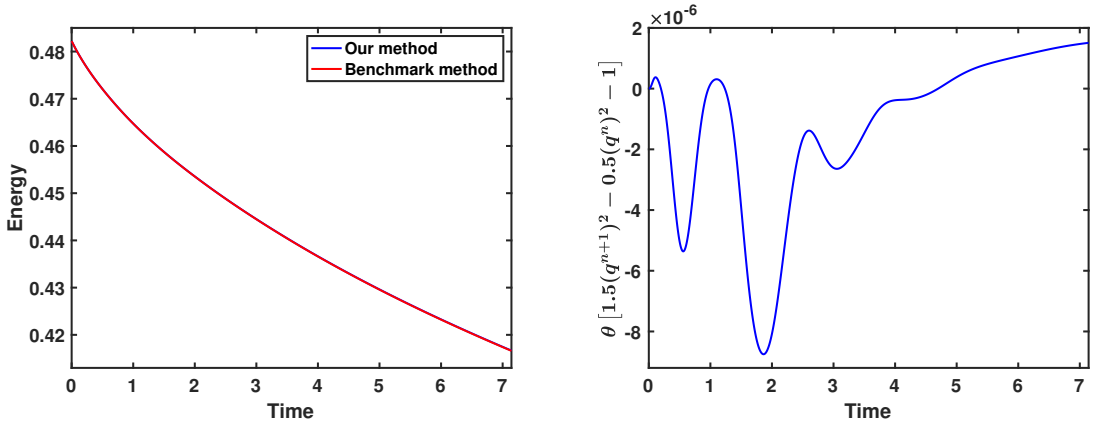

Figure 10: [Kelvin-Helmholtz instability, $Re = 100$] Evolution of the energy functional and error function $\mathcal{E}_2^n$ by the second-order DRLM scheme with $h = \frac{1}{256}$ and $\tau = \frac{1}{560}$.

Appendix A. Proof of energy stability for the first-order pressure-correction DRLM scheme (2.17)

Proof. Adding equations (2.17a) and (2.17b) together, noting that $\boldsymbol{f} = \boldsymbol{0}$, yields

$$\frac{\boldsymbol{u}^{n+1} - \boldsymbol{u}^n}{\tau} - \nu\Delta\overline{\boldsymbol{u}}^{n+1} + q^{n+1}\boldsymbol{F}(\boldsymbol{u}^n) + \nabla p^{n+1} = \boldsymbol{0}.$$

This implies that

$$\begin{aligned}\left(\frac{\boldsymbol{u}^{n+1} - \boldsymbol{u}^n}{\tau} + q^{n+1}\boldsymbol{F}(\boldsymbol{u}^n), \overline{\boldsymbol{u}}^{n+1}\right) &= \left(\nu\Delta\overline{\boldsymbol{u}}^{n+1} - \nabla p^{n+1}, \overline{\boldsymbol{u}}^{n+1}\right) \\ &= -\nu\left\|\nabla\overline{\boldsymbol{u}}^{n+1}\right\|^2 - \left(\nabla p^{n+1}, \overline{\boldsymbol{u}}^{n+1} - \boldsymbol{u}^{n+1}\right), \qquad \text{(A.1)}\end{aligned}$$

where in the last identity, we have used integration by parts and the fact that $\left(\nabla p^{n+1}, \boldsymbol{u}^{n+1}\right) = 0$ due to the incompressibility condition (2.17c). From (2.17b), we have $\overline{\boldsymbol{u}}^{n+1} - \boldsymbol{u}^{n+1} = \tau\nabla(p^{n+1} - p^n)$. Therefore, (A.1) can be written as

$$\begin{aligned}\left(\frac{\boldsymbol{u}^{n+1} - \boldsymbol{u}^n}{\tau} + q^{n+1}\boldsymbol{F}(\boldsymbol{u}^n), \overline{\boldsymbol{u}}^{n+1}\right) &= -\nu\left\|\nabla\overline{\boldsymbol{u}}^{n+1}\right\|^2 - \tau\left(\nabla p^{n+1}, \nabla(p^{n+1} - p^n)\right) \\ &= -\nu\left\|\nabla\overline{\boldsymbol{u}}^{n+1}\right\|^2 - \frac{\tau}{2}\left(\|\nabla p^{n+1}\|^2 - \|\nabla p^n\|^2 + \|\nabla(p^{n+1} - p^n)\|^2\right) \\ &\le -\frac{\tau}{2}\left(\|\nabla p^{n+1}\|^2 - \|\nabla p^n\|^2\right). \qquad \text{(A.2)}\end{aligned}$$

Combining (2.17d) and (A.2) gives us

$$\frac{\mathcal{K}(\boldsymbol{u}^{n+1}) - \mathcal{K}(\boldsymbol{u}^n)}{\tau} + \theta\frac{(q^{n+1})^2 - (q^n)^2}{\tau} \le -\frac{\tau}{2}\left(\|\nabla p^{n+1}\|^2 - \|\nabla p^n\|^2\right),$$

which leads to

$$\mathcal{K}(\boldsymbol{u}^{n+1}) + \frac{\tau^2}{2}\|\nabla p^{n+1}\|^2 + \theta(q^{n+1})^2 \le \mathcal{K}(\boldsymbol{u}^n) + \frac{\tau^2}{2}\|\nabla p^n\|^2 + \theta(q^n)^2.$$

Thus, (2.22) holds true for $0 \le n \le N_t - 1$. □

Appendix B. Proof of energy stability for the second-order rotational pressure-correction DRLM scheme (2.18)

Proof. Let $s^n := \nabla \cdot \sum_{i=1}^{n} \overline{\boldsymbol{u}}^i$ for $n \geq 1$, we have $\nabla \cdot \overline{\boldsymbol{u}}^{n+1} = s^{n+1} - s^n$. By taking the sum of equations (2.18a) and (2.18b), we obtain

$$\frac{3\boldsymbol{u}^{n+1} - 4\boldsymbol{u}^n + \boldsymbol{u}^{n-1}}{2\tau} - \nu\Delta\overline{\boldsymbol{u}}^{n+1} + q^{n+1}\boldsymbol{F}(\tilde{\boldsymbol{u}}^{n+1}) + \nabla(p^{n+1} + \nu s^{n+1} - \nu s^n) = \boldsymbol{0}.$$

It follows that

$$\begin{aligned}
&\left(\frac{3\boldsymbol{u}^{n+1} - 4\boldsymbol{u}^n + \boldsymbol{u}^{n-1}}{2\tau} + q^{n+1}\boldsymbol{F}(\tilde{\boldsymbol{u}}^{n+1}), \overline{\boldsymbol{u}}^{n+1}\right) \\
&= \left(\nu\Delta\overline{\boldsymbol{u}}^{n+1} - \nabla(p^{n+1} + \nu s^{n+1} - \nu s^n), \overline{\boldsymbol{u}}^{n+1}\right) \\
&= -\nu\|\nabla\overline{\boldsymbol{u}}^{n+1}\|^2 + \nu\left(\nabla s^n, \overline{\boldsymbol{u}}^{n+1}\right) - \left(\nabla(p^{n+1} + \nu s^{n+1}), \overline{\boldsymbol{u}}^{n+1} - \boldsymbol{u}^{n+1}\right),
\end{aligned} \tag{B.1}$$

where in the last equality, we have used integration by parts and the fact that $\left(\nabla(p^{n+1} + \nu s^{n+1}), \boldsymbol{u}^{n+1}\right) = 0$ due to (2.18c). It is implied from (2.18b) that

$$\overline{\boldsymbol{u}}^{n+1} - \boldsymbol{u}^{n+1} = \frac{2\tau}{3}\nabla(p^{n+1} + \nu s^{n+1} - p^n - \nu s^n). \tag{B.2}$$

The combination of (B.1) and (B.2) results in

$$\begin{aligned}
&\left(\frac{3\boldsymbol{u}^{n+1} - 4\boldsymbol{u}^n + \boldsymbol{u}^{n-1}}{2\tau} + q^{n+1}\boldsymbol{F}(\tilde{\boldsymbol{u}}^{n+1}), \overline{\boldsymbol{u}}^{n+1}\right) \\
&= -\nu\|\nabla\overline{\boldsymbol{u}}^{n+1}\|^2 + \nu\left(\nabla s^n, \overline{\boldsymbol{u}}^{n+1}\right) - \frac{2\tau}{3}\left(\nabla(p^{n+1} + \nu s^{n+1}), \nabla(p^{n+1} + \nu s^{n+1} - p^n - \nu s^n)\right).
\end{aligned} \tag{B.3}$$

Since $\nabla \cdot \overline{\boldsymbol{u}}^{n+1} = s^{n+1} - s^n$ and $\|\nabla \cdot \overline{\boldsymbol{u}}^{n+1}\| \leq \|\nabla\overline{\boldsymbol{u}}^{n+1}\|$, the second term on the right hand side of (B.3) can be estimated as

$$\begin{aligned}
\nu\left(\nabla s^n, \overline{\boldsymbol{u}}^{n+1}\right) &= -\nu(s^n, \nabla \cdot \overline{\boldsymbol{u}}^{n+1}) = -\nu(s^n, s^{n+1} - s^n) \\
&= -\frac{\nu}{2}\left(\|s^{n+1}\|^2 - \|s^n\|^2 - \|s^{n+1} - s^n\|^2\right) \\
&= -\frac{\nu}{2}\left(\|s^{n+1}\|^2 - \|s^n\|^2\right) + \frac{\nu}{2}\|\nabla \cdot \overline{\boldsymbol{u}}^{n+1}\|^2 \\
&\leq -\frac{\nu}{2}\left(\|s^{n+1}\|^2 - \|s^n\|^2\right) + \frac{\nu}{2}\|\nabla\overline{\boldsymbol{u}}^{n+1}\|^2.
\end{aligned} \tag{B.4}$$

Using the inequality $a(a-b) \geq \frac{1}{2}(a^2 - b^2)$, the last term on the right hand side of (B.3) can be bounded by

$$\begin{aligned}
&-\frac{2\tau}{3}\left(\nabla(p^{n+1} + \nu s^{n+1}), \nabla(p^{n+1} + \nu s^{n+1} - p^n - \nu s^n)\right) \\
&\leq -\frac{\tau}{3}\left(\left\|\nabla(p^{n+1} + \nu s^{n+1})\right\|^2 - \|\nabla(p^n + \nu s^n)\|^2\right).
\end{aligned} \tag{B.5}$$

From (B.3), (B.4), and (B.5), we derive

$$\begin{aligned}
&\left(\frac{3\boldsymbol{u}^{n+1}-4\boldsymbol{u}^{n}+\boldsymbol{u}^{n-1}}{2\tau}+q^{n+1}\boldsymbol{F}(\tilde{\boldsymbol{u}}^{n+1}),\overline{\boldsymbol{u}}^{n+1}\right)\\
&\leq-\frac{\nu}{2}\left(\|s^{n+1}\|^2-\|s^{n}\|^2\right)-\frac{\tau}{3}\left(\left\|\nabla(p^{n+1}+\nu s^{n+1})\right\|^2-\|\nabla(p^{n}+\nu s^{n})\|^2\right). \qquad \text{(B.6)}
\end{aligned}$$

Combining (2.18d) and (B.6) yields

$$\begin{aligned}
&\frac{3\mathcal{K}(\boldsymbol{u}^{n+1})-4\mathcal{K}(\boldsymbol{u}^{n})+\mathcal{K}(\boldsymbol{u}^{n-1})}{2\tau}+\theta\frac{3(q^{n+1})^2-4(q^{n})^2+(q^{n-1})^2}{2\tau}\\
&\leq-\frac{\nu}{2}\left(\|s^{n+1}\|^2-\|s^{n}\|^2\right)-\frac{\tau}{3}\left(\left\|\nabla(p^{n+1}+\nu s^{n+1})\right\|^2-\|\nabla(p^{n}+\nu s^{n})\|^2\right),
\end{aligned}$$

or equivalently,

$$\begin{aligned}
&\frac{3}{2}\mathcal{K}(\boldsymbol{u}^{n+1})-\frac{1}{2}\mathcal{K}(\boldsymbol{u}^{n})+\frac{\tau^2}{3}\left\|\nabla(p^{n+1}+\nu s^{n+1})\right\|^2+\frac{\tau\nu}{2}\|s^{n+1}\|^2+\theta\left[\frac{3}{2}(q^{n+1})^2-\frac{1}{2}(q^{n})^2\right]\\
&\leq\frac{3}{2}\mathcal{K}(\boldsymbol{u}^{n})-\frac{1}{2}\mathcal{K}(\boldsymbol{u}^{n-1})+\frac{\tau^2}{3}\left\|\nabla(p^{n}+\nu s^{n})\right\|^2+\frac{\tau\nu}{2}\|s^{n}\|^2+\theta\left[\frac{3}{2}(q^{n})^2-\frac{1}{2}(q^{n-1})^2\right].
\end{aligned}$$

Thus, we obtain (2.23) for $1\leq n\leq N_t-1$. □

CRediT authorship contribution statement

Cao-Kha Doan: Methodology, Software, Validation, Writing-original draft, Writing-reviewing and editing; **Thi-Thao-Phuong Hoang**: Conceptualization, Methodology, Project administration, Writing-reviewing and editing; **Lili Ju**: Conceptualization, Methodology, Writing-reviewing and editing; **Rihui Lan**: Validation, Writing-reviewing and editing.

Declaration of Interests

The authors have not disclosed any competing interests.

Data Availability

No data was used for the research described in the article.

Acknowledgements

T.-T.-P. Hoang's work is partially supported by U.S. National Science Foundation under grant number DMS-2041884. L. Ju's work is partially supported by U.S. National Science Foundation under grant numbers DMS-2109633 and DMS-2409634. R. Lan's work is partially supported by Shandong Provincial Natural Science Fund for Excellent Young Scientists Fund Program (Overseas) under grant number 2023HWYQ-064 and National Natural Science Foundation of China under grant number 12301531.

References

[1] Akrivis, G., Li, B. and Li, D., 2019. Energy-decaying extrapolated RK-SAV methods for the Allen-Cahn and Cahn-Hilliard equations. SIAM Journal on Scientific Computing, 41(6), pp.A3703-A3727.

[2] Albensoeder, S. and Kuhlmann, H.C., 2005. Accurate three-dimensional lid-driven cavity flow. Journal of Computational Physics, 206(2), pp.536-558.

[3] Benzi, M., Golub, G.H. and Liesen, J., 2005. Numerical solution of saddle point problems. Acta numerica, 14, pp.1-137.

[4] Chen, W., Jing, J., Liu, Q., Wang, C. and Wang, X., 2024. A second order numerical scheme of the Cahn-Hilliard-Navier-Stokes system with Flory-Huggins potential. Communications in Computational Physics, 35(3), pp.633-661.

[5] Chen, W., Liu, Y., Wang, C. and Wise, S., 2016. Convergence analysis of a fully discrete finite difference scheme for the Cahn-Hilliard-Hele-Shaw equation. Mathematics of Computation, 85(301), pp.2231-2257.

[6] Cheng, Q., Liu, C. and Shen, J., 2020. A new Lagrange multiplier approach for gradient flows. Computer Methods in Applied Mechanics and Engineering, 367, p.113070.

[7] Cheng, Q. and Wang, C., 2021. Error estimate of a second order accurate scalar auxiliary variable (SAV) numerical method for the epitaxial thin film equation. Adv. Appl. Math. Mech, 13(6), pp.1318-1354.

[8] Chorin, A.J., 1968. Numerical solution of the NS equations. Mathematics of computation, 22(104), pp.745-762.

[9] de Sturler, E. and Liesen, J., 2005. Block-diagonal and constraint preconditioners for nonsymmetric indefinite linear systems. Part I: Theory. SIAM Journal on Scientific Computing, 26(5), pp.1598-1619.

[10] DeCaria, V., Guzel, A., Layton, W. and Li, Y., 2021. A variable stepsize, variable order family of low complexity. SIAM Journal on Scientific Computing, 43(3), pp.A2130-A2160.

[11] Ghia, U.K.N.G., Ghia, K.N. and Shin, C.T., 1982. High-Re solutions for incompressible flow using the NS equations and a multigrid method. Journal of Computational Physics, 48(3), pp.387-411.

[12] Guermond, J.L., Minev, P. and Shen, J., 2006. An overview of projection methods for incompressible flows. Computer methods in applied mechanics and engineering, 195(44-47), pp.6011-6045.

[13] Guermond, J.L. and Shen, J., 2004. On the error estimates for the rotational pressure-correction projection methods. Mathematics of Computation, 73(248), pp.1719-1737.

[14] Guj, G. and Stella, F., 1993. A vorticity-velocity method for the numerical solution of 3D incompressible flows. Journal of Computational Physics, 106(2), pp.286-298.

[15] Hou, D. , Ning, Y. and Zhang, C., 2023. An efficient and robust Lagrange multiplier approach with a penalty term for phase-field models. Journal of Computational Physics, 488, 112236.

[16] Ji, B. and Liao, H.L., 2024. A unified L^2 norm error analysis of SAV-BDF schemes for the incompressible Navier–Stokes equations. Journal of Scientific Computing, 100(1), p.5.

[17] Jiang, B.N., Lin, T.L. and Povinelli, L.A., 1994. Large-scale computation of incompressible viscous flow by least-squares finite element method. Computer Methods in Applied Mechanics and Engineering, 114(3-4), pp.213-231.

[18] Jiang, M., Zhang, Z. and Zhao, J., 2022. Improving the accuracy and consistency of the scalar auxiliary variable (SAV) method with relaxation. Journal of Computational Physics, 456, p.110954.

[19] Ju, L. and Wang, Z., 2017. Exponential time differencing Gauge method for incompressible viscous flows. Communications in Computational Physics, 22(2), pp.517-541.

[20] Ku, H.C., Hirsh, R.S. and Taylor, T.D., 1987. A pseudospectral method for solution of the three-dimensional incompressible NS equations. Journal of Computational Physics, 70(2), pp.439-462.

[21] Li, X. and Rui, H., 2018. Superconvergence of characteristics marker and cell scheme for the Navier–Stokes equations on nonuniform grids. SIAM Journal on Numerical Analysis, 56(3), pp.1313-1337.

[22] Li, X. and Shen, J., 2020. Error analysis of the SAV-MAC scheme for the NS equations. SIAM Journal on Numerical Analysis, 58(5), pp.2465-2491.

[23] Li, X., Shen, J. and Liu, Z., 2022. New SAV-pressure correction methods for the NS equations: stability and error analysis. Mathematics of Computation, 91(333), pp.141-167.

[24] Lin, L., Yang, Z. and Dong, S., 2019. Numerical approximation of incompressible NS equations based on an auxiliary energy variable. Journal of Computational Physics, 388, pp.1-22.

[25] Liu, C., Frank, F., Alpak, F.O. and Rivière, B., 2019. An interior penalty discontinuous Galerkin approach for 3D incompressible Navier–Stokes equation for permeability estimation of porous media. Journal of Computational Physics, 396, pp.669-686.

[26] Liu, C., Ray, D., Thiele, C., Lin, L. and Riviere, B., 2022. A pressure-correction and bound-preserving discretization of the phase-field method for variable density two-phase flows. Journal of Computational Physics, 449, p.110769.

[27] Nochetto, R. and Pyo, J.H., 2005. Error estimates for semi-discrete gauge methods for the NS equations. Mathematics of computation, 74(250), pp.521-542.

[28] Orlando, G., Della Rocca, A., Barbante, P.F., Bonaventura, L. and Parolini, N., 2022. An efficient and accurate implicit DG solver for the incompressible Navier–Stokes equations. International Journal for Numerical Methods in Fluids, 94(9), pp.1484-1516.

[29] Oseledets, V.I., 1989. On a new way of writing the NS equation. The Hamiltonian formalism. Russ. Math. Surveys, 44, pp.210-211.

[30] Peyret, R. and Taylor, T.D., 2012. Computational methods for fluid flow. Springer Science & Business Media.

[31] Schroeder, P.W., John, V., Lederer, P.L., Lehrenfeld, C., Lube, G. and Schöberl, J., 2019. On reference solutions and the sensitivity of the 2D Kelvin–Helmholtz instability problem. Computers & Mathematics with Applications, 77(4), pp.1010-1028.

[32] Shen, J., Xu, J. and Yang, J., 2018. The scalar auxiliary variable (SAV) approach for gradient flows. Journal of Computational Physics, 353, pp.407-416.

[33] Shen, J., Xu, J. and Yang, J., 2019. A new class of efficient and robust energy stable schemes for gradient flows. SIAM Review, 61(3), pp.474-506.

[34] Temam, R., 1969. Sur l'approximation de la solution des équations de NS par la méthode des pas fractionnaires (II). Archive for rational mechanics and analysis, 33, pp.377-385.

[35] Wang, M., Huang, Q. and Wang, C., 2021. A second order accurate scalar auxiliary variable (SAV) numerical method for the square phase field crystal equation. Journal of Scientific Computing, 88(2), p.33.

[36] Wang, C. and Liu, J.G., 2000. Convergence of gauge method for incompressible flow. Mathematics of computation, 69(232), pp.1385-1407.

[37] Wang, C., Wang, J., Xia, Z. and Xu, L., 2022. Optimal error estimates of a second-order projection finite element method for magnetohydrodynamic equations. Mathematical Modeling and Numerical Analysis, 56(3), pp.767-789.

[38] Weinan, E. and Liu, J.G., 1995. Projection method I: convergence and numerical boundary layers. SIAM journal on numerical analysis, pp.1017-1057.

[39] Weinan, E. and Liu, J.G., 2000. Gauge finite element method for incompressible flows, Int. J. Num. Meth. Fluids, 34, pp.701–710.

[40] Weinan, E. and Liu, J.G., 2003. Gauge method for viscous incompressible flows. Communications in Mathematical Sciences, 1(2), pp.317-332.

[41] Wong, K.L. and Baker, A.J., 2002. A 3D incompressible Navier–Stokes velocity–vorticity weak form finite element algorithm. International Journal for Numerical Methods in Fluids, 38(2), pp.99-123.

[42] Yang, X., 2016. Linear, first and second-order, unconditionally energy stable numerical schemes for the phase field model of homopolymer blends. Journal of Computational Physics, 327, pp.294-316.

[43] Yang, X. and Ju, L., 2017. Efficient linear schemes with unconditional energy stability for the phase field elastic bending energy model. Computer Methods in Applied Mechanics and Engineering, 315, pp.691-712.

[44] Yang, J., Tan, Z. and Kim, J., 2022. Original variables based energy-stable time-dependent auxiliary variable method for the incompressible Navier–Stokes equation. Computers & Fluids, 240, p.105432.

[45] Yang, X., Zhao, J. and Wang, Q., 2017. Numerical approximations for the molecular beam epitaxial growth model based on the invariant energy quadratization method. Journal of Computational Physics, 333, pp.104-127.

[46] Yang, X., Zhao, J., Wang, Q. and Shen, J., 2017. Numerical approximations for a three-component Cahn–Hilliard phase-field model based on the invariant energy quadratization method. Mathematical Models and Methods in Applied Sciences, 27(11), pp.1993-2030.